FDA-MIMO Transceiver Design Under the Uniform Frequency Increment Constraint

Lan Lan, *Member, IEEE*, Massimo Rosamilia, *Member, IEEE*, Augusto Aubry, *Senior Member, IEEE*, Antonio De Maio, *Fellow, IEEE*, and Guisheng Liao, *Senior Member, IEEE*

***Abstract*— This paper investigates the joint optimization of transmit parameters and receive filter in a Frequency Diverse Array (FDA)-Multiple-Input Multiple-Output (MIMO) radar system with a uniform frequency increment from sensor to sensor. The problem is formulated as the maximization of the Signal-to-Interference-plus-Noise Ratio (SINR) at the output of the receive filter in a signal-dependent clutter environment, taking into account some practical constraints on the probing waveform and frequency increment. To tackle the resulting non-convex and NP-hard optimization problem, a Minorization-Maximization (MM)-Maximum Block Improvement (MBI) algorithm is developed, which iteratively updates the variables block that yields the maximum increase of the objective function while keeping the others fixed. The convergence properties of the proposed algorithm are rigorously studied, and the computational complexity is analyzed. Numerical results demonstrate the effectiveness of the designed procedure under several clutter scenarios of practical relevance, including proper comparisons with counterparts.**

***Index Terms*— FDA-MIMO radar, frequency optimization, waveform design, signal-dependent clutter, MM-MBI, KKT condition.**

I. Introduction

NOWADAYS, radar systems are experiencing a revolutionary transformation through tailored waveform design, a powerful tool that paved the way to remarkable performance enhancement in challenging operating conditions characterized by signal-dependent clutter environments [1], [2]. In the open literature, the optimization of the output Signal-to-Interference-plus-Noise Ratio (SINR) at the receive filter stands out as the main goal, and it is usually tackled by exploiting some possible *a priori* knowledge of the target and environment [3], [4]. However, fulfilling this task demands overcoming some challenges, in terms of constraints in the optimization process, stemming from practical requirements and limitations. The most interesting include constant modulus code, the use of discrete phase alphabet, limits to the Peak-to-Average-power Ratio (PAR), finite energy, and total transmit power, as well as guaranteeing waveform similarity with a particular reference signal [5], [6], [7], [8], [9], [10]. Given that the resulting design demands generally the solution of a non-convex and NP-hard optimization problem, several approaches have been successfully employed to yield high-quality waveforms synthesis. These methods include Majorization-Minimization (MM) [11], Cyclic Algorithms (CA) [12], [13], Alternating Direction Method of Multipliers (ADMM) [14], [15], successive Quadratically Constrained Quadratic Programming (QCQP) refinement [9], and Coordinate Descent (CD) paradigms [16], [17].

While the majority of works in the open literature have predominantly concentrated on waveform design with phased arrays and/or MIMO systems, leveraging the spatial degrees of freedom (DOF) available for interference suppression and improved detection performance, it is important to note that there has been a growing interest in Frequency Diverse Arrays (FDA) and FDA-MIMO systems [18], [19], [20], [21], [22]. As a matter of fact, capitalizing on the range-angle-dependent beampattern characteristic of this type of transceivers, several applications have been proposed in the open literature, such as the adaptive target detection [19], multi-dimensional parameter estimation [23], mainlobe deceptive jammer suppression [24], range-ambiguous clutter suppression [25], as well as Synthetic Aperture Radar (SAR) imaging [26]. Notably, the carrier frequency of each transmit element represents an additional Degrees-Of-Freedom (DOF) of these sensing systems, which could be suitably optimized to further improve the radar performance [27], [28], [29]. In [30], the joint transmit and receive weights optimization for a coherent FDA system is proposed to maximize the power toward the desired two-dimensional range-angle cell. The target localization problem for a possibly cognitive FDA radar is addressed in [31] by optimizing the transmit signal parameters. In [32], the transmit beamspace and receive filter of an FDA-MIMO radar are optimized to maximize the SINR at the radar receiver end. Moreover, in the context of moving target detection, a cognitive design of transmitter and receive filter

Manuscript received 5 February 2024; revised 5 April 2024; accepted 8 April 2024. Date of publication 12 April 2024; date of current version 29 April 2024. The work of Lan Lan and Guisheng Liao was supported in part by the National Natural Science Foundation of China under Grants 62101402 and 61931016 and in part by the Science and Technology Innovation Team of Shaanxi Province under Grant 2022TD-38. The work of Massimo Rosamilia, Augusto Aubry, and Antonio De Maio was partially supported by the European Union under the Italian National Recovery and Resilience Plan (NRRP) of NextGenerationEU, partnership on "Telecommunications of the Future" (PE00000001 - program "RESTART") *(Corresponding author: Antonio De Maio.)*

Lan Lan and Guisheng Liao are with the National Key Laboratory of Radar Signal Processing, Xidian University, Xi'an 710071, China (e-mail: lanlan@xidian.edu.cn; liaogs@xidian.edu.cn).

Massimo Rosamilia, Augusto Aubry, and Antonio De Maio are with DIETI, University of Naples Federico II, 80125 Naples, Italy, and also with the National Inter-University Consortium for Telecommunications, 43124 Parma, Italy (e-mail: massimo.rosamilia@unina.it; augusto.aubry@unina.it; ademaio@unina.it).

Digital Object Identifier 10.1109/TRS.2024.3388212

for an FDA-MIMO radar is investigated in [33]. An optimal FDA-MIMO frequency design scheme is proposed in [34] to improve the localization estimation accuracy, exploiting prior knowledge on potential target locations. However, the joint optimization of both the frequency increment, radar code, and receiver filter has only received a limited attention. Noteworthy, in [35], the FDA-MIMO radar parameters are optimized considering arbitrary frequency increments (unstructured case). However, the situation of equal frequency increment (structured case) represents an architecture of greater practical relevance. This is due to its relatively simple implementation, as it demands only a single oscillator and a sequence of frequency multipliers, in contrast to a more general case requiring multiple oscillators, which are not only more costly but also pose synchronization and phase noise challenges. Given these guidelines, this work develops a joint design strategy of both the transmit parameters (i.e., the frequency increment/radar code) and the receive filter in an FDA-MIMO radar, aimed at improving the SINR at the receiver end, thereby boosting the detection performance. To this end, proper knowledge of the signal-dependent clutter statistics, provided by (possibly dynamically updated) site specific environmental databases, is suitably exploited to accurately model the received signal at the Cell Under Test (CUT). Thus, the optimization problem is formulated by maximizing the SINR w.r.t. the transmitter and receiver parameters. Furthermore, to endow practical appealing to the design, constraints on the energy of the code and its similarity with a bespoke probing waveform, along with limitations on frequency increment that account for the available radar bandwidth, have also been carefully included in the optimization process [4], [35]. Within this context, a tailored Minorization-Maximization (MM)-Maximum Block Improvement (MBI) procedure [35] has been devised to address the NP-hard non-convex optimization problem at hand. Consequently, the main contributions of this paper can be summarized as follows.

- After modeling the signal from the CUT as the superposition of target echo, clutter samples, and thermal noise, a SINR optimization problem is formulated capitalizing on *a priori* knowledge on the clutter statistics and including the aforementioned constraints on the frequency increment and radar code.
- A MM-MBI solution strategy is devised to tackle the optimization problem by iteratively optimizing each variables block. In particular, at each iteration, three subproblems w.r.t. the receive filter, radar code, and frequency increment (keeping the other variable fixed), are either optimally solved exploiting hidden convexities, or handled resorting to the MM paradigm (for the frequency increment optimization). Then, only the block yielding the maximum increase of the output SINR is updated, until reaching a steady condition.
- The convergence properties of the devised algorithm are rigorously studied. Precisely, any cluster point of the sequence generated by the procedure satisfies the Karush-Kuhn-Tucker (KKT) conditions for the problem [36]. This is also complemented with a thoroughly discussion on the computational complexity of the method.
- Numerical results are illustrated to assess the capability of the devised transceiver optimization process under diverse clutter scenarios of practical relevance, where appropriate comparisons among the alternating optimization (AO) procedure, the MM-MBI in [35], and other simpler MBI-based optimization strategies (also considering the MIMO configuration) are included to highlight the effectiveness of the proposed strategy.

The paper is organized as follows. In Section II, the signal model of FDA-MIMO radar (under the uniform frequency increment constraint) in the presence of signal-dependent clutter is introduced. In Section III, the problem of joint transmitter and receiver optimization is formulated, and the MM-MBI algorithm is proposed to tackle the constrained optimization problem. In addition, the convergence properties and the computational complexity of the devised strategy are thoroughly discussed. Numerical results are presented in Section IV, whereas conclusions and possible future research avenues are provided in Section V.

A. Notations

Boldface is used for vectors $\boldsymbol{a}$ (lower case), and matrices $\boldsymbol{A}$ (upper case). The (k,l)-entry (or l-entry) of a generic matrix $\boldsymbol{A}$ (or vector $\boldsymbol{a}$) is indicated as $\boldsymbol{A}(k,l)$ (or a_l). $\boldsymbol{I}$ and $\boldsymbol{0}$ denote respectively the identity matrix and the matrix with zero entries (their size is determined from the context). The all-ones column vector of size N is denoted by $\mathbf{1}_N$, whereas $\boldsymbol{e}_k$ denotes the k-th column vector of $\boldsymbol{I}$, whose size is determined from the context. Additionally, $\mathrm{diag}(\boldsymbol{x})$ indicates the diagonal matrix whose i-th diagonal element is $\boldsymbol{x}(i)$. The transpose and the conjugate transpose operators are denoted by the symbols $(\cdot)^{\mathrm{T}}$ and $(\cdot)^{\dagger}$, respectively. $\odot$, and $\otimes$ represent the Hadamard (element-wise) product, and Kronecker product, respectively. $\mathbb{R}^N$ and $\mathbb{C}^N$ are respectively the sets of N-dimensional column vectors of real and complex numbers. The letter j refers to the imaginary unit (i.e., $j=\sqrt{-1}$). For any complex number x, $|x|$ indicates the modulus of x and $\mathrm{Re}\{x\}$ denotes its real part. Moreover, for any $\boldsymbol{x}\in\mathbb{C}^N$, $\|\boldsymbol{x}\|$ denotes the Euclidean norm. $\mathbb{E}[\cdot]$ denotes the statistical expectation. Furthermore, for any $x, y\in\mathbb{R}$, $\max(x,y)$ returns the maximum between the two arguments. Finally, for any optimization problem $\mathcal{P}$, $\upsilon(\mathcal{P})$ represents its optimal value.

II. System Model of Linear FDA-MIMO Radar

Let us consider an FDA-MIMO system comprising two subarrays with M transmit and N receive antenna elements, respectively, arranged in a Uniform Linear Array (ULA) configuration (as depicted in Fig.1). Considering the frequency of each transmit element linearly increasing from a reference carrier f_0 with step Δf, the actual carrier frequency of the m-th ($m=1,\ldots,M$) transmit element is given by

$$f_m = f_0 + (m-1)\Delta f. \tag{1}$$

Assuming that the array elements transmit orthogonal waveforms, a common code sequence (referred to as a radar

TABLE I
DEFINITIONS OF THE MODEL PARAMETERS

Parameter	Definition	Parameter	Definition
α_0	complex coefficient of the useful received signal $\boldsymbol{z}_{\rm S}$ [19]	$t^\star$	sampling instant
$\tau_0 = 2R_0/c$	envelope time delay	$\Delta\tau = t^\star - \tau_0$	incremental delay [19]
d	array interelement spacing	λ_0	reference carrier wavelength
$2L-2,\ L \le P$	number of range rings that interfere with the Bin-Of-Interest (BOI), i.e., $(l,i)=(0,0)$	I	number of discrete azimuth sectors [37]
K	maximum number of scatterers within a single range-azimuth bin	θ_i	azimuth of the i-th $(i=1,\ldots,I)$ sector
$\Delta\tau_k$	incremental delay of the k-th $(k=1,\ldots,K)$ scatterer from the i-th $(i=1,\ldots,I)$ azimuth sector	$\beta_{l,i,k}$	amplitude of the k-th scatterer from the (l,i)-th range-azimuth bin

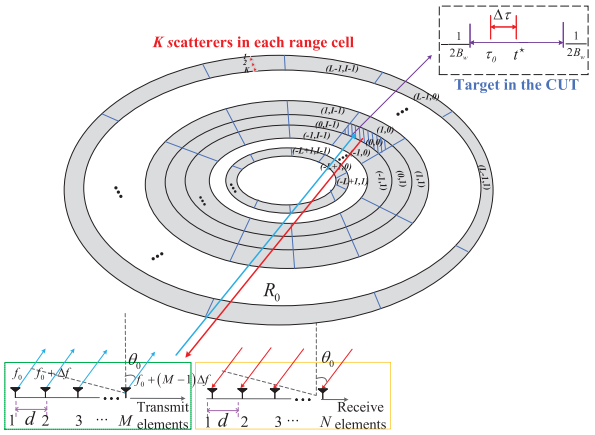

Fig. 1. Geometry of the FDA and range-azimuth bins contributing to the return from the CUT.

code) of length $P \ge 3$, i.e., $\boldsymbol{c} = [c_1, c_2, \ldots, c_P]^{\rm T} \in \mathbb{C}^P$, is used to modulate the fast-time transmitted signals.

At the receiver end, the impinging signals undergo down-conversion, matched filtering, and sampling to produce a PMN-dimensional vector $\boldsymbol{v} \in \mathbb{C}^{PMN}$ that represents the fast-time observations from the range-azimuth CUT. In the presence of a target in the far field with an azimuth angle of θ_0 and a distance of R_0 from the receiver, the received signal resulting from the CUT can be modeled as [4]

$$\boldsymbol{v} = \boldsymbol{z}_{\rm S} + \boldsymbol{z}_{\rm C} + \boldsymbol{n}, \tag{2}$$

where (see Table I for the model parameters definition)

- $\boldsymbol{z}_{\rm S} = \alpha_0 \boldsymbol{c} \otimes \boldsymbol{s}(\theta_0, \Delta\tau, \Delta f) \in \mathbb{C}^{PMN}$ denotes the vector of the samples from the target echo, with $\boldsymbol{s}(\theta_0, \Delta\tau, \Delta f) = \boldsymbol{d}(\theta_0) \otimes \left[\boldsymbol{a}(\theta_0) \odot \boldsymbol{b}(\Delta\tau, \Delta f)\right] \in \mathbb{C}^{MN}$ the joint transmit-receive steering vector [23] with
  - $\boldsymbol{d}(\theta_0) = \left[1, e^{j2\pi \frac{d}{\lambda_0}\sin(\theta_0)}, \cdots, e^{j2\pi \frac{d}{\lambda_0}(N-1)\sin(\theta_0)}\right]^{\rm T} \in \mathbb{C}^N$ the angle-dependent receive steering vector;
  - $\boldsymbol{a}(\theta_0) = \left[1, e^{j2\pi \frac{d}{\lambda_0}\sin(\theta_0)}, \cdots, e^{j2\pi \frac{d}{\lambda_0}(M-1)\sin(\theta_0)}\right]^{\rm T} \in \mathbb{C}^M$ the angle-dependent transmit steering vector;
  - $\boldsymbol{b}(\Delta\tau, \Delta f) = \left[1, e^{j2\pi\Delta\tau\Delta f}, \ldots, e^{j2\pi\Delta\tau(M-1)\Delta f}\right]^{\rm T} \in \mathbb{C}^M$ the range-dependent transmit steering vector;
- $\boldsymbol{z}_{\rm C}$

$$= \sum_{l=-L+1}^{L-1} \sum_{i=0}^{I-1} \sum_{k=1}^{K} \beta_{l,i,k} \boldsymbol{J}_l \boldsymbol{c} \otimes \boldsymbol{s}(\theta_i, \Delta\tau_k, \Delta f) \in \mathbb{C}^{PMN} \tag{3}$$

contains the filtered clutter samples from the range-azimuth bins adjacent to the CUT (as depicted in Fig. 1), which is the superposition of the returns from different uncorrelated scatterers,[1] with $\boldsymbol{J}_l \in \mathbb{R}^{P\times P}$ the binary shift matrix with ones only on its l-th ($l = 0, \pm1, \pm2, \ldots, \pm(P-1)$) diagonal ($l$ indicates the range ring), and zeros elsewhere, i.e.,

$$\boldsymbol{J}_l(p,q) = \begin{cases} 1, & p-q=l \\ 0, & \text{elsewhere,} \end{cases} \quad (p,q) \in \{1,\ldots,P\}^2, \tag{4}$$

with $\boldsymbol{J}_0 = \boldsymbol{I}$. As a result, the covariance matrix of $\boldsymbol{z}_{\rm C}$ is given by

$$\begin{aligned} \boldsymbol{\Sigma}_{\rm c}(\boldsymbol{c}, \Delta f) &= \mathbb{E}[\boldsymbol{z}_{\rm C}\boldsymbol{z}_{\rm C}^\dagger] \\ &= \sum_{l=-P+1}^{P-1} \sum_{i=0}^{I-1} \sum_{k=1}^{K} \sigma_{l,i,k}^2 \bar{\boldsymbol{\Gamma}}_l(\boldsymbol{c}, \theta_i, \Delta\tau_k, \Delta f) \\ &\quad \in \mathbb{C}^{PMN\times PMN}, \end{aligned} \tag{5}$$

with $\bar{\boldsymbol{\Gamma}}_l(\boldsymbol{c}, \theta_i, \Delta\tau_k, \Delta f) \in \mathbb{C}^{PMN\times PMN}$ given by

$$\begin{aligned} &\bar{\boldsymbol{\Gamma}}_l(\boldsymbol{c}, \theta_i, \Delta\tau_k, \Delta f) \\ &= \left(\boldsymbol{J}_l \boldsymbol{c}\boldsymbol{c}^\dagger \boldsymbol{J}_l^\dagger\right) \otimes \left(\boldsymbol{s}(\theta_i, \Delta\tau_k, \Delta f)\boldsymbol{s}^\dagger(\theta_i, \Delta\tau_k, \Delta f)\right); \end{aligned} \tag{6}$$

- $\boldsymbol{n} \in \mathbb{C}^{PMN}$ represents the thermal noise contribution, modeled as a zero-mean, complex, circularly symmetric, random vector, i.e., $\mathbb{E}[\boldsymbol{n}] = 0$, with covariance matrix $\mathbb{E}[\boldsymbol{n}\boldsymbol{n}^\dagger] = \sigma_n^2 \boldsymbol{I}$ and noise power level σ_n^2 assumed, without loss of generality, equal to 0 dB.

Before concluding this section, it is worth mentioning that the model could also be extended to account for the presence of stand-off noise-like jammers, via a signal-independent covariance term (generally non-diagonal), as well as the case of self-screening deception jamming interferences, where each return resembles that of a clutter patch.

III. JOINT TRANSMIT AND RECEIVE FILTER DESIGN PROBLEM

In this section, a method for jointly optimizing the FDA-MIMO radar DOFs (radar code/frequency increment) and receive filter is proposed. Specifically, by processing the collected signal $\boldsymbol{v}$ using the weight vector $\boldsymbol{w} \in \mathbb{C}^{PMN}$, the

[1]The amplitude returns of the clutter scatterers are modeled as independent complex, zero-mean, circularly symmetric, random variables with $\mathbb{E}[|\beta_{l,i,k}|^2] = \sigma_{l,i,k}^2$. Moreover, $\beta_{l,i,k} = 0\ \forall k$ when $l = 0$ and $i = 0$.

SINR (normalized with respect to (w.r.t.) $|\alpha_0|^2$) downstream the receive filter is given by

$$\mathrm{SINR}(\boldsymbol{w}, \boldsymbol{c}, \Delta f) = \frac{|\boldsymbol{w}^\dagger(\boldsymbol{c} \otimes \boldsymbol{s}(\theta_0, \Delta\tau, \Delta f))|^2}{\boldsymbol{w}^\dagger \boldsymbol{\Sigma}_c(\boldsymbol{c}, \Delta f)\boldsymbol{w} + \sigma_n^2 \|\boldsymbol{w}\|^2}. \tag{7}$$

Now, aimed at maximizing (7), the following transceiver design problem is formulated, i.e.,

$$\mathcal{P}: \begin{cases} \max\limits_{\boldsymbol{c}, \boldsymbol{w}, \Delta f} & \mathrm{SINR}(\boldsymbol{w}, \boldsymbol{c}, \Delta f) \\ \text{s.t.} & 0 \le (M-1)\Delta f \le B_w \\ & \|\boldsymbol{c}\|^2 = 1 \\ & \|\boldsymbol{c} - \boldsymbol{c}_0\|^2 \le \delta \\ & \|\boldsymbol{w}\|^2 = 1, \end{cases} \tag{8}$$

which accounts for several constraints[2] on the optimizing parameters stemming from physical limitations and desirable behaviors:

- frequency increment constraint: given the available radar bandwidth B_w, the frequency increment should satisfy:

$$0 \le (M-1)\Delta f \le B_w, \tag{9}$$

  where B_w denotes the available radar bandwidth for the total carrier offset and $B_w + B_c$ the overall single-side radar bandwidth with B_c the sub-pulse bandwidth;
- code constraints: to comply with the radar power budget, the energy constraint is forced on the radar code to account for the finite energy transmitted by the system, which is tantamount to forcing

$$\|\boldsymbol{c}\|^2 = 1. \tag{10}$$

  In addition, to bestow some desirable attributes to the radar probing code, a similarity constraint is imposed on the transmitted sequence, i.e.,

$$\|\boldsymbol{c} - \boldsymbol{c}_0\|^2 \le \delta, \tag{11}$$

  where $0 < \delta < 2$ rules the size of the similarity region, and $\boldsymbol{c}_0 \in \mathbb{C}^P$ represents a reference code ($\|\boldsymbol{c}_0\| = 1$), which possesses some desired features from the radar performance point of view (as for instance limited amplitude variation among the elements).

It is now worth noting that obtaining the global optimal solution to $\mathcal{P}$ is generally a difficult task for which analytic closed-form solution could not be available. More specifically, since $\mathcal{P}$ is a non-convex and NP-hard optimization problem, the development of a reduced-complexity (practically implementable) sub-optimal solution strategy holding some optimality features is demanded. This motivates the design of the proposed MM-MBI optimization algorithm [5], [37], [38], [39], capable of providing good-quality solutions with affordable computational complexity. Precisely, at each iteration, the method locally optimizes (possibly using the MM paradigm) each variables block, i.e., frequency increment, radar code, or filter, and evaluate the corresponding SINR increment. Then, it updates only the variables block yielding the maximum increment and proceeds with the next iteration, until reaching convergence. In order to formally describe the procedure, let us introduce the vector $\boldsymbol{y}$ collecting all the optimization variables, i.e.,

$$\boldsymbol{y} = \left[\boldsymbol{w}^{\mathrm{T}}, \boldsymbol{c}^{\mathrm{T}}, \Delta f\right]^{\mathrm{T}} \in \mathbb{C}^{PMN+P+1}, \tag{12}$$

which is partitioned into 3 blocks given by $\boldsymbol{y}_1, \boldsymbol{y}_2, y_3$, with $\boldsymbol{y}_1 = \boldsymbol{w} \in \mathbb{C}^{PMN}$, $\boldsymbol{y}_2 = \boldsymbol{c} \in \mathbb{C}^P$, and $y_3 = \Delta f$ corresponding to the receive filter, radar code, and frequency increment to be optimized, respectively. Moreover, the optimization vector obtained at the n-th iteration is denoted by

$$\boldsymbol{y}^n = \left[\boldsymbol{w}^{(n)\mathrm{T}}, \boldsymbol{c}^{(n)\mathrm{T}}, \Delta f^{(n)}\right]^{\mathrm{T}}. \tag{13}$$

As previously mentioned, the procedure demands the optimization of each variables block at time, while keeping the others fixed [37]. Formally, at each iteration, it requires the solutions to the following subproblems (or appropriate surrogate variants):

$$\mathcal{P}_{\Delta f^{(n)}}: \begin{cases} \max\limits_{\Delta f} & \mathrm{SINR}\left(\boldsymbol{w}^{(n-1)}, \boldsymbol{c}^{(n-1)}, \Delta f\right) \\ \text{s.t.} & 0 \le (M-1)\Delta f \le B_w, \end{cases} \tag{14}$$

$$\mathcal{P}_{\boldsymbol{c}^{(n)}}: \begin{cases} \max\limits_{\boldsymbol{c}} & \mathrm{SINR}\left(\boldsymbol{w}^{(n-1)}, \boldsymbol{c}, \Delta f^{(n-1)}\right) \\ \text{s.t.} & \|\boldsymbol{c}\|^2 = 1 \\ & \|\boldsymbol{c} - \boldsymbol{c}_0\|^2 \le \delta, \end{cases} \tag{15}$$

and

$$\mathcal{P}_{\boldsymbol{w}^{(n)}}: \begin{cases} \max\limits_{\boldsymbol{w}} & \mathrm{SINR}\left(\boldsymbol{w}, \boldsymbol{c}^{(n-1)}, \Delta f^{(n-1)},\right) \\ \text{s.t.} & \|\boldsymbol{w}\|^2 = 1. \end{cases} \tag{16}$$

Then, based on the output value of (14)-(16), the MBI rule updates the variable yielding the maximum SINR.

From an analytical point of view, $\Delta f^{(n)}$, $\boldsymbol{c}^{(n)}$, and $\boldsymbol{w}^{(n)}$ are suitable feasible points (either optimal or bespoke sub-optimal) to the sub-problems $\mathcal{P}_{\Delta f^{(n)}}$, $\mathcal{P}_{\boldsymbol{c}^{(n)}}$, and $\mathcal{P}_{\boldsymbol{w}^{(n)}}$, respectively.

A solution strategy to solve $\mathcal{P}_{\Delta f^{(n)}}$ is presented in Subsection III-A by means of the MM approach. As to Problems $\mathcal{P}_{\boldsymbol{c}^{(n)}}$ and $\mathcal{P}_{\boldsymbol{w}^{(n)}}$, since they are hidden convex, an optimal solution to $\mathcal{P}_{\boldsymbol{c}^{(n)}}$ can be found in polynomial-time [4] (see Subsection III-B), whereas an optimal solution to problem $\mathcal{P}_{\boldsymbol{w}^{(n)}}$ is available in closed form (see Section III-C).

A. Frequency Increment Optimization

In this subsection, the frequency increment Δf is optimized given the receive filter and the radar code. Before proceeding further, it is important to highlight that the main difference with [35] lies in the frequency optimization stage. In particular, the optimization strategy in [35] involves M sub-problems, related to the unstructured frequency increment of each array element. In contrast, the scenario of equal frequency increments (1) is here considered. Consequently, for a given code and filter, only the frequency increment Δf must be optimized. To proceed further, the following Lemma is introduced, which provides an alternative expression of the objective SINR in (7).

[2]Being the objective function scale invariant, without loss of generality, the unit norm constraint on the filter vector can be added.

Lemma 1: An equivalent expression of the objective function in (14) is

$$\mathrm{SINR}\left(\boldsymbol{w}^{(n-1)}, \boldsymbol{c}^{(n-1)}, \Delta f\right) = \frac{\boldsymbol{b}_0^{\dagger}(\Delta f)\boldsymbol{W}\left(\boldsymbol{w}^{(n-1)}, \boldsymbol{c}^{(n-1)}\right)\boldsymbol{b}_0(\Delta f)}{\sum_{k=1}^{K}\boldsymbol{b}_k^{\dagger}(\Delta f)\boldsymbol{\Sigma}_k\left(\boldsymbol{w}^{(n-1)}, \boldsymbol{c}^{(n-1)}\right)\boldsymbol{b}_k(\Delta f) + \sigma_n^2\|\boldsymbol{w}^{(n-1)}\|^2}, \tag{17}$$

where

$$\boldsymbol{b}_0(\Delta f) = \boldsymbol{b}(\Delta\tau, \Delta f), \qquad \boldsymbol{b}_k(\Delta f) = \boldsymbol{b}(\Delta\tau_k, \Delta f) \tag{18}$$

$$\boldsymbol{W}\left(\boldsymbol{w}^{(n-1)}, \boldsymbol{c}^{(n-1)}\right) = \boldsymbol{H}^{\dagger}\boldsymbol{w}^{(n-1)}\boldsymbol{w}^{(n-1)\dagger}\boldsymbol{H} \in \mathbb{C}^{M\times M} \tag{19}$$

with

$$\boldsymbol{H} = \boldsymbol{c}^{(n-1)} \otimes \boldsymbol{d}(\theta_0) \otimes \mathrm{diag}(\boldsymbol{a}(\theta_0)) \in \mathbb{C}^{PMN\times M}, \tag{20}$$

whereas

$$\boldsymbol{\Sigma}_k\left(\boldsymbol{w}^{(n-1)}, \boldsymbol{c}^{(n-1)}\right) = \sum_{l=-P+1}^{P-1}\sum_{i=0}^{I-1}\sigma_{l,i,k}^2\hat{\boldsymbol{w}}_{l,i}\hat{\boldsymbol{w}}_{l,i}^{\dagger} \in \mathbb{C}^{M\times M} \tag{21}$$

with

$$\hat{\boldsymbol{w}}_{l,i} = \left(\boldsymbol{J}_l\boldsymbol{c}^{(n-1)} \otimes \boldsymbol{d}(\theta_i) \otimes \mathrm{diag}(\boldsymbol{a}(\theta_i))\right)^{\dagger}\boldsymbol{w}^{(n-1)} \in \mathbb{C}^{M}. \tag{22}$$

Proof: The proof follows the same line of reasoning as in [35, Appendix A], using the range-dependent steering vector $\boldsymbol{b}(\Delta\tau, \Delta f)$ (structured case) in lieu of $\boldsymbol{b}(\Delta\tau, \widetilde{\boldsymbol{\Delta f}}_m)$ for the unstructured architecture. ∎

In order to tackle the sub-problem at hand, a MM approach is developed, whereby an appropriate tight minorant to the objective function at hand (constructed according to Proposition 1) is optimized to generate an updated solution.

Proposition 1: A tight minorant (surrogate) to the objective function in $\mathcal{P}_{\Delta f^{(n)}}$ is given by

$$\widehat{\mathrm{SINR}}_a\left(\Delta f|\Delta f^{(n-1)}, \boldsymbol{w}^{(n-1)}, \boldsymbol{c}^{(n-1)}\right) = X^{(n-1)}\Delta f^2 + \dot{\hat{X}}^{(n-1)}\Delta f + \ddot{\hat{X}}^{(n-1)}, \tag{23}$$

with the specific definitions of $X^{(n-1)}$, $\dot{\hat{X}}^{(n-1)}$, and $\ddot{\hat{X}}^{(n-1)}$ reported in Appendix A.

Proof: The interested reader may refer to Appendix A. ∎

By leveraging Proposition 1, at the n-th iteration, the devised MM-MBI procedure demands solving

$$\mathcal{P}_{y_3^{(n)}}: \begin{cases} \max\limits_{y_3} \ \widehat{\mathrm{SINR}}_a\left(y_3|y_3^{(n-1)}, \boldsymbol{w}^{(n-1)}, \boldsymbol{c}^{(n-1)}\right) \\ \text{s.t.} \quad y_3 \in \Psi \end{cases}, \tag{24}$$

where the feasible set Ψ is given by

$$\Psi = \{x : 0 \le x \le B_w/(M-1)\}. \tag{25}$$

That said, a feasible solution to (24) is provided by the following proposition.

Proposition 2: The optimal solution to $\mathcal{P}_{y_3^{(n)}}$ is

$$\hat{y}_3 = \max(\min(\tilde{y}_3, B_w/(M-1)), 0) \tag{26}$$

with

$$\tilde{y}_3 = -\frac{\dot{\hat{X}}^{(n-1)}}{2X^{(n-1)}}. \tag{27}$$

Proof: See Appendix B. ∎

Hence, starting from $\Delta f^{(n-1)}$, $\boldsymbol{w}^{(n-1)}$, and $\boldsymbol{c}^{(n-1)}$, the optimization of y_3 can be accomplished according to (26).

B. Radar Code Optimization

In this subsection, the radar code is optimized considering the frequency increment Δf and the receive filter as fixed parameters, set to the values at the previous iteration. First of all, using the following lemma, an equivalent form of the objective function in (15) is obtained.

Lemma 2: An equivalent expression of the objective function in (15) is

$$\mathrm{SINR}\left(\boldsymbol{w}^{(n-1)}, \boldsymbol{c}, \Delta f^{(n-1)}\right) = \frac{\boldsymbol{c}^{\dagger}\boldsymbol{\Theta}\left(\boldsymbol{w}^{(n-1)}, \Delta f^{(n-1)}\right)\boldsymbol{c}}{\boldsymbol{c}^{\dagger}\boldsymbol{M}\left(\boldsymbol{w}^{(n-1)}, \Delta f^{(n-1)}\right)\boldsymbol{c}}. \tag{28}$$

where

- $\boldsymbol{\Theta}(\boldsymbol{w}^{(n-1)}, \Delta f^{(n-1)}) = \boldsymbol{S}^{\dagger}\boldsymbol{w}^{(n-1)}\boldsymbol{w}^{(n-1)\dagger}\boldsymbol{S} \in \mathbb{C}^{P\times P}$ with $\boldsymbol{S} = \boldsymbol{I}_P \otimes \boldsymbol{s}(\theta_0, \Delta\tau, \Delta f^{(n-1)}) \in \mathbb{C}^{PMN\times P}$;
- $\boldsymbol{M}(\boldsymbol{w}^{(n-1)}, \Delta f^{(n-1)}) = \boldsymbol{\Phi}(\boldsymbol{w}^{(n-1)}, \Delta f^{(n-1)}) + \sigma_n^2\boldsymbol{I} \in \mathbb{C}^{P\times P}$ with $\boldsymbol{\Phi}(\boldsymbol{w}^{(n-1)}, \Delta f^{(n-1)}) = \sum_{l=-P+1}^{P-1}\sum_{i=0}^{I-1}\sum_{k=1}^{K}\sigma_{l,i,k}^2\boldsymbol{J}_l^{\dagger}\bar{\boldsymbol{S}}_{i,k}^{\dagger}\boldsymbol{w}^{(n-1)}\boldsymbol{w}^{(n-1)\dagger}\bar{\boldsymbol{S}}_{i,k}\boldsymbol{J}_l \in \mathbb{C}^{P\times P}$ and $\bar{\boldsymbol{S}}_{i,k} = \boldsymbol{I}_P \otimes \boldsymbol{s}(\theta_i, \Delta\tau_k, \Delta f^{(n-1)}) \in \mathbb{C}^{PMN\times P}$.

Proof: The proof follows the Appendix D in [35], where the single increment Δf is considered in lieu of the vector of frequencies $\boldsymbol{\Delta f}$.

In this regard, the problem $\mathcal{P}_{\boldsymbol{c}^{(n)}}$ is recast as

$$\mathcal{P}_{\boldsymbol{y}_2^{(n)}}: \begin{cases} \max\limits_{\boldsymbol{y}_2} \ \mathrm{SINR}\left(\boldsymbol{y}_1^{(n-1)}, \boldsymbol{y}_2, y_3^{(n-1)}\right) \\ \text{s.t.} \quad \|\boldsymbol{y}_2\|^2 = 1 \\ \qquad \|\boldsymbol{y}_2 - \boldsymbol{c}_0\|^2 \le \delta \end{cases}, \tag{29}$$

which is a fractional quadratic optimization problem, whose optimal solution is denoted in the following as $\hat{\boldsymbol{y}}_2$.

The solution technique employed to solve (29) is detailed in [35], which demands solving a relaxed SDP problem (dropping the rank-one constraint) and then computing the radar code accounting for the performed Charnes and Cooper's transformation and specific rank-one decompositions [4], [40], [41].

C. Receive Filter Optimization

By considering the transmitter parameters fixed at their values at the current iteration, the filter (here denoted by the variable $\boldsymbol{y}_1$) at the n-th iteration can be updated by solving the following optimization problem

$$\mathcal{P}_{\boldsymbol{y}_1^{(n)}}: \begin{cases} \max\limits_{\boldsymbol{y}_1} \ \mathrm{SINR}(\boldsymbol{y}_1, \boldsymbol{y}_2^{(n-1)}, y_3^{(n-1)}) \\ \text{s.t.} \quad \|\boldsymbol{y}_1\|^2 = 1 \end{cases}. \tag{30}$$

The optimal solution to $\mathcal{P}_{\boldsymbol{y}_1^{(n)}}$ is obtained according to [4] and [42], and it is given in (31), as shown at the bottom of the next page.

D. Joint Transmit and Receive Optimization Procedure

The joint transmit and receive optimization process is summarized in **Algorithm 1**, where a suitable initialization of the radar code and the frequency increment, i.e., $\boldsymbol{y}_2^{(0)} = \boldsymbol{c}_0$,

Algorithm 1 Joint Transmit and Receive Optimization With MM-MBI

Input: M, $\sigma_{l,i,k}^2$, $\boldsymbol{c}_0$, δ, B_w, σ_n^2, N_1.
Output: $\boldsymbol{y}^\star$.

Initialization:

- Set $n = 0$;
- Set $\boldsymbol{y}_1^{(0)}$ as the RHS of (31) with $\boldsymbol{y}_2^{(n-1)} = \boldsymbol{y}_2^{(0)}$ and $y_3^{(n-1)} = y_3^{(0)}$;
- Set $\boldsymbol{y}_2^{(0)} = \boldsymbol{c}_0$;
- Set $y_3^{(0)} = B_w/(M-1)$;
- Define $\boldsymbol{y}^{(0)} = \left[\boldsymbol{y}_1^{(0)\mathrm{T}}, \boldsymbol{y}_2^{(0)\mathrm{T}}, y_3^{(0)}\right]^{\mathrm{T}}$;
- Evaluate $\chi(\boldsymbol{y}^{(0)})$;

repeat

3. $n = n + 1$;
4. for $h = 1, 2, 3$, let $v_h^{(n)}$ and $\hat{\boldsymbol{y}}_h$ be, respectively, the optimal value and an optimal solution to $\mathcal{P}_{\boldsymbol{y}_h^{(n)}}$;
5. Compute $k^\star = \arg\max_{k=1,2,3} v_k^{(n)}$;
6. Let $\boldsymbol{y}_h^{(n)} = \boldsymbol{y}_h^{(n-1)}$ for all $h \neq k^\star$ and $\boldsymbol{y}_{k^\star}^{(n)} = \hat{\boldsymbol{y}}_{k^\star}$
7. Define $\boldsymbol{y}^{(n)} = \left[\boldsymbol{y}_1^{(n)\mathrm{T}}, \boldsymbol{y}_2^{(n)\mathrm{T}}, y_3^{(n)}\right]^{\mathrm{T}}$;
8. Compute $\chi(\boldsymbol{y}^{(n)})$;

until $|\chi(\boldsymbol{y}^{(n)}) - \chi(\boldsymbol{y}^{(n-1)})| < \varepsilon_1$.
Output $\boldsymbol{y}^\star = \boldsymbol{y}^{(n)}$.

$y_3^{(0)} = B_w/(M-1)$, is employed to compute the optimal filter $\boldsymbol{y}_1^{(0)}$. Therefore, the process to update the frequency increment, radar code, and receive filter, could be iteratively repeated for a desired number of iterations $N_1 > 0$ or when reaching a convergence condition, e.g.,

$$\left|\chi\left(\boldsymbol{y}^{(n)}\right) - \chi\left(\boldsymbol{y}^{(n-1)}\right)\right| < \varepsilon_1,$$

where $\varepsilon_1 > 0$ is the user-defined threshold, and $\chi(\boldsymbol{y}^{(n)})$ is the objective function (7) evaluated at $\boldsymbol{y}^{(n)} = \left[\boldsymbol{y}_1^{(n)\mathrm{T}}, \boldsymbol{y}_2^{(n)\mathrm{T}}, y_3^{(n)}\right]^{\mathrm{T}}$.

A schematic representation of the proposed joint transmit-receive optimization procedure is reported Fig. 2, where the clutter statistics are provided by (possibly dynamically updated) site specific environmental databases, such as Geographical Information System (GIS), digital terrain maps, meteorological information, and clutter models [4]. Remarkably, accurate and timely clutter information is crucial for maximizing the actual SINR at the receiver end by designing bespoke filter (receiver side), radar code and frequency increment (transmitter side).

As a matter of fact, the devised framework could be easily conceived as part of a general cognitive process where a perception stage, i.e., a continuous sensing of the environment (to extract clutter statistics) is iteratively alternated to the system action, i.e., where the radar transmits a fast-time signal that maximizes the actual SINR. Precisely, this is achieved by

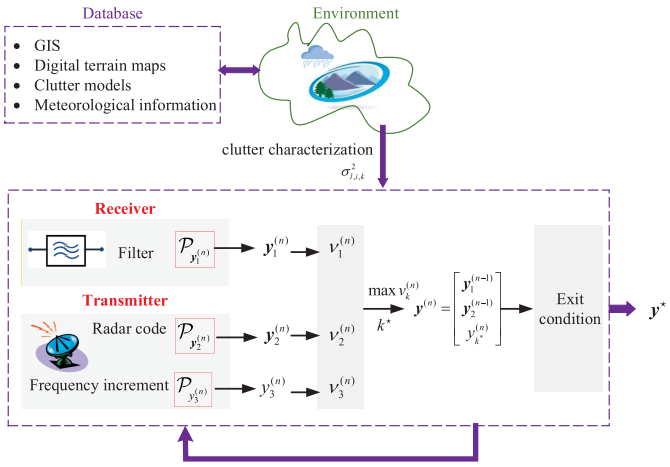

Fig. 2. Block diagram of the transmit-receive optimization procedure.

modulating the signal with the optimized radar code and using the FDA-MIMO tuned to the computed frequency increment. Given the memory access latency and the computation time of the cognitive algorithm, it is necessary to know the status of the surveilled region after a time interval Δt (look-ahead processing paradigm). Moreover, if Δt is greater than the memory access latency and the processing time, the cognitive system is physically implementable [43], [44].

As to the convergence analysis, some relevant properties of the optimization problem $\mathcal{P}$ and **Algorithm 1** are summarized in Proposition 3.

Proposition 3: The optimization problem $\mathcal{P}$ enjoys the following properties:

- The objective $\chi(\boldsymbol{y})$ is a continuous function and the feasible set is compact. Thus, according to the Weierstrass theorem, $\mathcal{P}$ is solvable, i.e., there exists at least a global maximum point of SINR$(\boldsymbol{w}, \boldsymbol{c}, \Delta f)$; as a consequence $\chi(\boldsymbol{y}^{(n)}) \leq \upsilon(\mathcal{P})$;
- The objective $\chi(\boldsymbol{y}^{(n)})$ is monotonically increasing and converges to a finite value $\chi^\star$. Moreover, for any cluster point $\boldsymbol{y}^\star$ of $\boldsymbol{y}^{(n)}$, $\chi(\boldsymbol{y}^\star) = \chi^\star$;
- Any cluster point $\boldsymbol{y}^\star$ satisfies the KKT conditions for Problem $\mathcal{P}$.

Proof: See Appendix C. ∎

It is worth noting that Problem $\mathcal{P}$ can be also handled by resorting to the AO framework [37]. Following this approach, an optimization algorithm for the joint transmit and receiver design could be obtained, whose main difference with **Algorithm 1** is the update rule. In particular, the MBI approach demands the optimization of each variables block and the update at each iteration corresponds to the variables block yielding the maximum SINR improvement; conversely, with the AO framework, each variables block is cyclically optimized at each iteration. Notably, this AO process

$$\hat{\boldsymbol{y}}_1 = \frac{(\boldsymbol{\Sigma}_c(\boldsymbol{y}_2^{(n-1)}, y_3{}^{(n-1)}) + \sigma_n^2\boldsymbol{I})^{-1}(\boldsymbol{y}_2^{(n-1)} \otimes \boldsymbol{s}(\theta_0, \Delta\tau, y_3{}^{(n-1)}))}{\sqrt{(\boldsymbol{y}_2^{(n-1)} \otimes \boldsymbol{s}(\theta_0, \Delta\tau, y_3{}^{(n-1)}))^\dagger(\boldsymbol{\Sigma}_c(\boldsymbol{y}_2^{(n-1)}, y_3{}^{(n-1)}) + \sigma_n^2\boldsymbol{I})^{-2}(\boldsymbol{y}_2^{(n-1)} \otimes \boldsymbol{s}(\theta_0, \Delta\tau, y_3{}^{(n-1)}))}}, \tag{31}$$

enjoys the same properties as the first and second items of Proposition 3. However, the KKT condition cannot be ensured (in general) for any cluster point $\boldsymbol{y}^{\star}$.

Before concluding this section, the computational complexity of **Algorithm 1** is investigated. In particular, the evaluation of the optimized frequency increment (step 4), radar code (step 5), and receive filter (step 5), are detailed in the following.

- Computing the optimal solution to the Problem $\mathcal{P}_{y_3^{(n)}}$ demands $\mathcal{O}(KIPM^2)$, due to the computation of the K matrices $\boldsymbol{\Sigma}_k\left(\boldsymbol{w}^{(n-1)}, \boldsymbol{c}^{(n-1)}\right)$.
- To update the radar code, it is first necessary to solve the SDP problem $\hat{\mathcal{P}}_{\boldsymbol{y}_2^{(n)}}$, which requires $\mathcal{O}(P^{3.5}\log(1/\eta))$ operations, with η a predefined accuracy [4], [45]. This step will also yield the optimal value to the corresponding problem. Then, the synthesis of the code via the rank-one decomposition demands $\mathcal{O}(P^3)$ [41].
- The optimal receive filter evaluation is dominated by the computation of $\boldsymbol{\Sigma}_c(\boldsymbol{y}_2^{(n-1)}, \Delta f^{(n-1)})$, which is $\mathcal{O}(P^3M^2N^2IK)$, and the inverse of $\boldsymbol{\Sigma}_c(\boldsymbol{y}_2^{(n-1)}, \Delta f^{(n-1)}) + \sigma_n^2\boldsymbol{I}$, which is $\mathcal{O}((PMN)^3)$. Therefore the overall computational complexity is $\mathcal{O}(P^3M^2N^2(KI + MN))$. However, since it is positive definite, after the computation of $\boldsymbol{\Sigma}_c(\boldsymbol{y}_2^{(n-1)}, \boldsymbol{\Delta f}^{(n-1)})$, the filter could be efficiently computed resorting to the Conjugate Gradient Method (CGM) [46], with a resulting computational saving.

Consequently, the overall computational complexity of each iteration in **Algorithm 1** is $\mathcal{O}(P^{3.5}\log(1/\eta) + P^3M^2N^2(KI + MN))$.

Moreover, it is worth noting that the computational burden of some MBI iterations can be mitigated by avoiding redundant evaluations of some terms. For example, the value of $\boldsymbol{\Sigma}_c(\boldsymbol{c}^{(n-1)}, \Delta f^{(n-1)})$ can be reused (storing it in memory) until the code or the frequency increment is reoptimized. Similarly, the computation of $\boldsymbol{\Sigma}_k\left(\boldsymbol{w}^{(n-1)}, \boldsymbol{c}^{(n-1)}\right)$, $k = 1, \ldots, K$ is demanded only after the optimization of the filter or the code. Indeed, for the same number of iterations, empirical simulations have shown that specific optimization patterns (in terms of MBI selections) can sometimes lead to a computational saving in the MM-MBI implementation as compared to the MM-AO counterpart, due to the larger number of redundant calculations avoided in the former procedure.

Finally, it is worth considering the possibility of parallelizing, at each iteration of the MM-MBI procedure, the optimization of the filter, the code, and the frequency increment, to further reduce the overall computational time.

IV. Performance Analysis

This section investigates the performance of the devised optimization scheme in terms of achieved SINR. To this end, a FDA-MIMO radar, equipped with two ULAs (one for transmission and the other for reception) having $M = 4$ and $N = 8$ elements, respectively, with an inter-element distance of half-wavelength, is considered. In addition, the transmitting array elements are supposed to radiate orthogonal baseband signals at carrier frequency $f_0 = 1$ GHz. Furthermore, for the procedure execution, a standard Barker code of length $P = 11$ is used as reference radar code, i.e.,

$$\boldsymbol{c}_0 = [1, 1, 1, -1, -1, -1, 1, -1, -1, 1, -1]^{\mathrm{T}}, \tag{32}$$

with similarity parameter $\delta = 0.5$, and available radar bandwidth $B_w = 2$ MHz are supposed.

TABLE II
Simulation Parameters of FDA-MIMO Radar

Parameter	Value	Parameter	Value
M	4	N	8
Δf	0.5 MHz	B_w	2 MHz
I	181	L	11
u_0	0	$\Delta\tau_0$	$0.1\mu s$
σ_n^2	0 dB	B	1 MHz
K	5	P	11

In the following, two different scenarios are envisaged, characterized by the presence of both clutter edges and heterogeneous clutter patches. Notably, the clutter statistical characterization is supposed to be known *a priori*, e.g., obtained by means of a site specific environment database system [4], as mentioned before. Furthermore, the parameters employed for the simulations are listed in Table I.

To assess the capabilities of the devised approach, at each iteration, the SINR achieved with the MM-MBI and MM-AO strategies is compared with

- MBI optimizing only the transmitted code and the receive filter[3] (referred to as MBI-C&F), namely $\boldsymbol{w}$ and $\boldsymbol{c}$ are obtained from

$$\mathcal{P}_{\boldsymbol{w},\boldsymbol{c}}: \begin{cases} \max\limits_{\boldsymbol{w},\boldsymbol{c}} \ \mathrm{SINR}(\boldsymbol{w}, \boldsymbol{c}, \Delta f^{(0)}) \\ \text{s.t.} \quad \|\boldsymbol{w}\|^2 = 1 \\ \qquad \|\boldsymbol{c}\|^2 = 1 \\ \qquad \|\boldsymbol{c} - \boldsymbol{c}_0\|^2 \le \delta \end{cases}; \tag{33}$$

  as well as the MBI optimization for the MIMO configuration (referred to as MBI-MIMO), i.e., solving (33) with $\Delta f^{(0)} = 0$.
- MBI optimizing only the frequency increment and the receive filter (referred to as MBI-DF&F), namely $\boldsymbol{w}$ and Δf are obtained from

$$\mathcal{P}_{\boldsymbol{w},\Delta f}: \begin{cases} \max\limits_{\boldsymbol{w},\Delta f} \ \mathrm{SINR}(\boldsymbol{w}, \boldsymbol{c}_0, \Delta f) \\ \text{s.t.} \quad \|\boldsymbol{w}\|^2 = 1 \\ \qquad 0 \le \Delta f \le B_w/(M-1), \end{cases}, \tag{34}$$

- the optimal receive filter (referred to as OPT-FLT), i.e.,

$$\begin{aligned} \boldsymbol{w}_{OPT-FLT} &= \arg\max_{\boldsymbol{w}} \mathrm{SINR}(\boldsymbol{w}, \boldsymbol{c}_0, \Delta f^{(0)}) \\ &\text{s.t. } \|\boldsymbol{w}\|^2 = 1 \end{aligned} \tag{35}$$

  computed as the RHS of (31) with $n = 1$, $\boldsymbol{y}_2^{(0)} = \boldsymbol{c}_0$, $y_3^{(0)} = \Delta f^{(0)}$.
- MM-MBI optimizing the transmitted radar code, frequency increments for each element of the transmit array, and receive filter (referred to as MBI-all), whose design

[3]As there are only two optimization blocks in problems (33) and (34), the MBI and AO represent equivalent solution strategies.

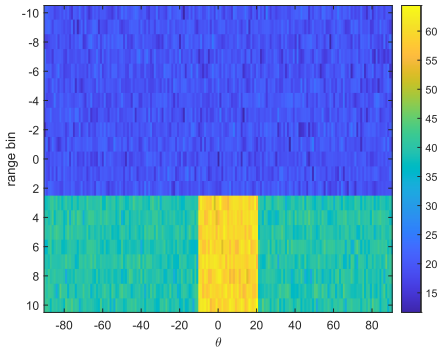

Fig. 3. Clutter power distribution (dB) of considered in Section IV-A, i.e., an heterogeneous environment with clutter edges.

problem is given by [35]

$$\mathcal{P}_{\boldsymbol{c},\boldsymbol{w},\Delta f}: \begin{cases} \max\limits_{\substack{\boldsymbol{c},\boldsymbol{w},\\ \Delta f_1,\ldots,\Delta f_M}} & \mathrm{SINR}(\boldsymbol{w},\boldsymbol{c},\Delta f) \\ \text{s.t.} & 0 \le \Delta f_m \le B_w \\ & m = 1,\ldots,M \\ & \|\boldsymbol{c}\|^2 = 1 \\ & \|\boldsymbol{c}-\boldsymbol{c}_0\|^2 \le \delta \\ & \|\boldsymbol{w}\|^2 = 1 \end{cases}, \tag{36}$$

where Δf_m denotes the frequency increments (w.r.t. f_0) related to the m-th transmit element.

- MBI for Problem (36) initialized with the results of the proposed MM-MBI method, which will be referred to as MBI-double.

A. Heterogeneous Environment With Clutter Edges

The first case study considers an heterogeneous clutter environment encompassing clutter edges as illustrated in Fig. 3, which reports the clutter power $\bar{\sigma}^2_{l,i}$ at each range-azimuth bin, given by the sum of the mean square values of the K clutter scatterers from the (l,i)-th range-azimuth bin, i.e.,

$$\bar{\sigma}^2_{l,i} = \mathrm{CNR}_{l,i} \sum_{k=1}^{K} |\eta_{l,i,k}|^2 \tag{37}$$

where $\eta_{l,i,k}$ is a zero-mean, unit-variance, complex Gaussian random variable and $\mathrm{CNR}_{l,i} = 10\mathrm{dB}$ in the range rings from -11 to 2, while for the other rings the clutter profile is considered having $\mathrm{CNR}_{l,i} = 50$ dB within the region $[-10°, 20°]$ and $\mathrm{CNR}_{l,i} = 30$ dB elsewhere. In addition, no clutter is supposed in the BOI, i.e., $\eta_{0,0,k} = 0$, $k = 1, \ldots, K$, whose return is associated with target echo sought in that range-azimuth bin.

Fig. 4 reports the SINR (versus iteration) achieved by the aforementioned optimization processes. Inspection of the curves in Fig. 4 (a) reveals that both the proposed MM-MBI and MM-AO algorithms are capable of significantly improving the SINR with a resulting gain of 5.69 dB as compared with the initial SINR. Notably, the two methods yield similar results (with a slight advantage of the MM-MBI approach) after 100 iterations, whereas for a very small number of iterations, the MM-AO-based optimization outperforms its counterpart. Moreover, the MM-MBI achieves noticeable performance

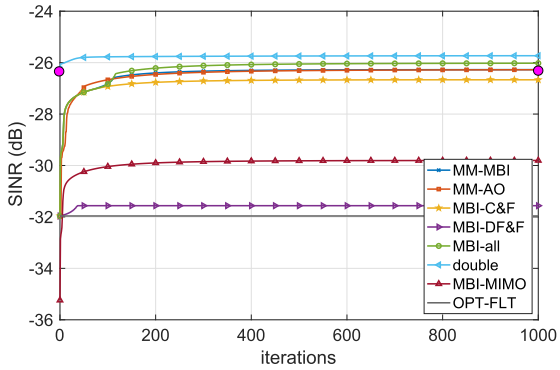

(a)

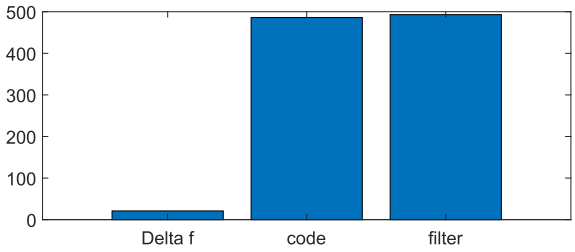

(b)

Fig. 4. Optimization results for the first environmental scenario: (a) Normalized SINR versus the number of iterations; (b) Number of times each parameter is optimized using the proposed MBI-based algorithm. The magenta circles indicate a SINR of -26.27 dB.

improvement over the MBI-C&F, MBI-DF&F, and MBI-MIMO approaches, with gaps in the order of 0.39 dB, 5.29 dB, and 3.53 dB, respectively, at the 1000-th iteration. Not surprisingly, by optimizing the frequency increment of each transmit element (the curve labeled MBI-all), a slight improvement (in the order of 0.3 dB) can be attained over the proposed methods, with the disadvantage of a more complex hardware architecture as well as a more computationally demanding procedure (due to the enlarged search space). In addition, by initializing this procedure with the outcomes of the devised MM-MBI algorithm at the 1000-th iteration (whose achieved SINR value is indicated with a magenta circle in Fig. 4 (a)), it is possible to get a further performance boost (the curve labeled double) over the MBI-all counterpart in less than 100 iterations. Consequently, in a scenario where the carrier frequency of each transmitting element can be optimized, the MM-MBI method can be also effectively employed to provide a high-quality initialization leading to a fast achievement (in terms of the total number of optimization problems solved) of the steady state. Furthermore, Fig. 4 (b) reports the number of times each variables block is optimized by the MBI selection strategy, highlighting the key role of the code and filter optimization (over the frequency increment) for this clutter scenario.

The range-angle system response is reported in Fig. 5, that is

$$|\boldsymbol{w}^{(n)\dagger}\boldsymbol{v}_{l,i}|^2,\ l = -L+1,\ldots,L-1,\ i = 0,\ldots,I-1 \tag{38}$$

with $\boldsymbol{v}_{l,i} = \boldsymbol{J}_l\boldsymbol{c}^{(n)} \otimes \boldsymbol{s}(\theta_i, \Delta\tau_k, \Delta f^{(n)})$ corresponding to the strength of filter output to an echo return located at θ_i and l-th range ring, with the optimized code and frequency increment

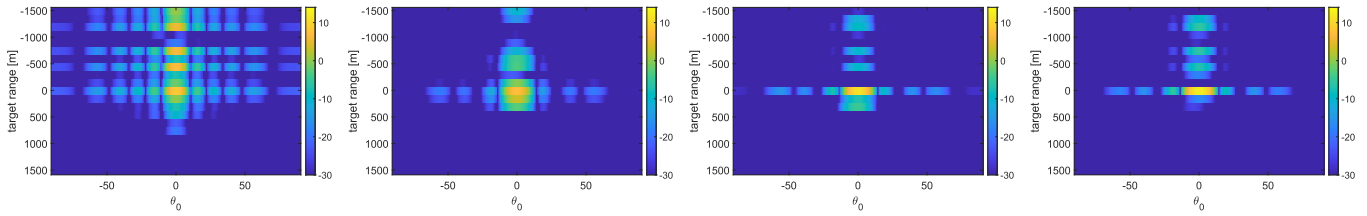

Fig. 5. Squared modulus (dB) of the filter response at a given range-azimuth position for the first environmental scenario and iteration: (a) Initial; (b) 4-th iteration; (c) 100-th iteration; (d) 1000-th iteration.

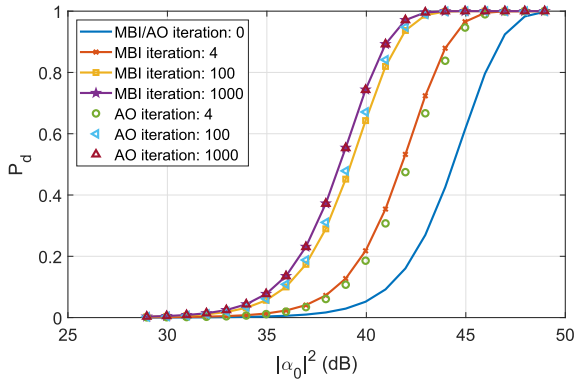

Fig. 6. Detection probability at a given iteration for the first environmental scenario.

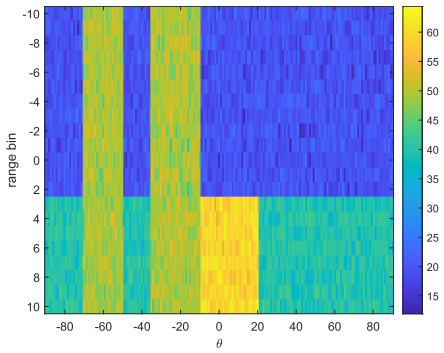

Fig. 7. Clutter power distribution (dB) of Section IV-B, i.e., an heterogeneous environment with clutter edges and range-patches.

at: (a) initialization, (b) 4-th, (c) 100-th, and (d) 1000-th iterations of the MM-MBI algorithm, which are respectively shown in Figs. 5 (a)-(d). The results highlight the performance improvement obtained by the MM-MBI strategy over the several iterations, with the results of focusing the energy at the target's bin, i.e., 0° and $L = 0$, while suppressing the echoes located at other azimuth-range pairs, clearly confirming the performance benefits offered by the joint transmit-receive optimization for clutter suppression.

As a further analysis to corroborate the performance increment from a radar detection standpoint, the target detection results are examined considering the case of non-fluctuating (Swerling 0) target, with the coherent detector designed as

$$|\hat{\boldsymbol{w}}^{\dagger}\boldsymbol{v}| \underset{\mathcal{H}_1}{\overset{\mathcal{H}_0}{\gtrless}} \zeta, \tag{39}$$

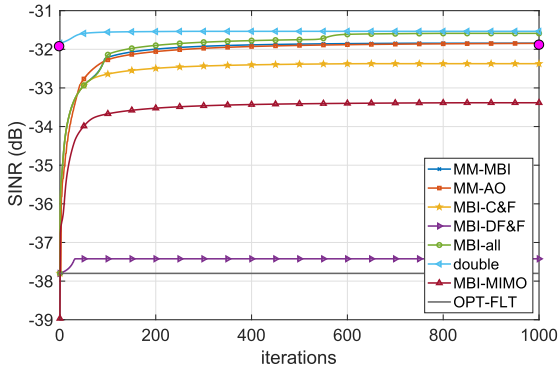

(a)

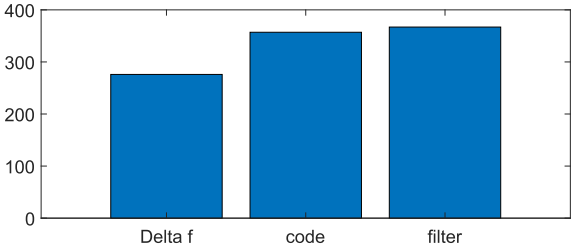

(b)

Fig. 8. Optimization results for the second environmental scenario: (a) Normalized SINR versus the number of iterations; (b) Number of times each parameter is optimized using the proposed MBI-based algorithm. The magenta circles indicate a SINR of −31.84 dB.

where $\mathcal{H}_0$ and $\mathcal{H}_1$ indicate the null and the alternative hypothesis (i.e., target echo absence/presence within the received observation vector), respectively, and ζ is the detection threshold set to ensure the desired false alarm probability (P_{fa}). Hence, under the Gaussian assumption for the interference, the probability of detection ($\mathrm{P_d}$) is obtained via

$$Q\left(\sqrt{2|\alpha_0|^2\chi}, \sqrt{-2\ln P_{fa}}\right) \tag{40}$$

where $Q(\cdot)$ is the Marcum Q function [47], $\hat{\boldsymbol{w}}$ is the optimized received filter, and χ is the SINR achieved after the joint transmit-receive optimization.

The $\mathrm{P_d}$ versus $|\alpha_0|^2$, for $P_{fa} = 10^{-4}$, at different iterations of the devised MM-MBI procedure, is reported in Fig. 6 assuming the same clutter environment as in Fig. 3. The results show that, for a given $|\alpha_0|^2$, an increase in the number of iterations of the MBI/AO-based procedures is connected to better $\mathrm{P_d}$ values. Additionally, the MM-MBI approach yields a small performance improvement over the MM-AO counterpart,

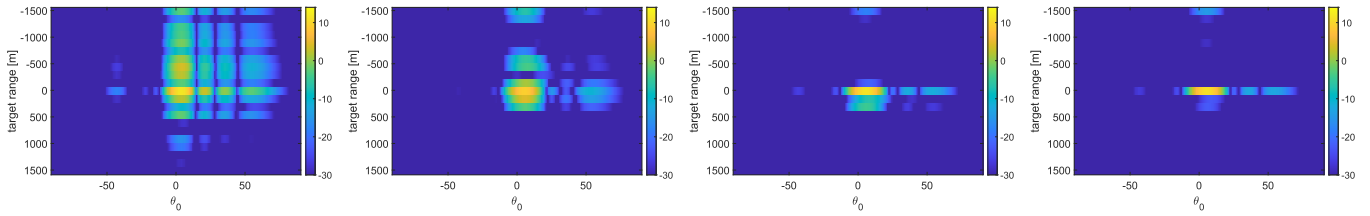

Fig. 9. Squared modulus (dB) of the filter response at a given range-azimuth position for the second environmental scenario and iteration: (a) Initial; (b) 4-th iteration; (c) 100-th iteration; (d) 1000-th iteratio.

just after 4 iterations. Nevertheless, the gap between their curves reduces as the number of iterations increases, leading to a negligible displacement by the 1000-th iteration.

B. Mixed Heterogeneous Environment With Clutter Patches and Edges

As second case study, a mixed clutter profile is considered (whose power distribution is depicted in Fig. 10), characterized by clutter patches and edges. Precisely, two range-patches are simulated respectively in the regions of $[-70°, -50°]$ with $\text{CNR}_1 = 40$ dB and $[-35°, -10°]$ with $\text{CNR}_2 = 40$ dB. Moreover, in angular sectors different from the patches, there are clutter edges as in the previous case study, i.e., with $\text{CNR}_1 = 10$dB from range rings -11 to 2, whereas in the other rings $\text{CNR}_2 = 50$ dB for the region $[-10°, 20°]$, and $\text{CNR}_3 = 30$ dB elsewhere.

The SINR performance of all considered methodologies is illustrated in Fig. 8 (a). The plot shows that, likewise the previous scenario, MM-MBI and MM-AO achieve similar performance and obtain a gain of 5.96 dB at the 1000-th iteration. In addition, by optimizing all the frequencies of the transmit elements, the procedure yields a further SINR increment of 0.5 dB compared with MM-MBI. Notably, such a value can be obtained in just 50 iterations if the procedure is initialized with the outcomes of the proposed (and less computationally demanding) MM-MBI approach at the 1000-th iteration. Moreover, the SINR improvement obtained by the MBI-C&F and the MBI-MIMO rank second and third, with a gap of 0.5 dB and 1.54 dB, respectively, as compared with the MM-MBI. In addition, the MBI-DF&F is unable to provide satisfactory SINR improvement due to the absence of code optimization, thereby highlighting the key roles of both transmitter parameters (i.e., code and frequency increment) and receive filter optimizations.

Interestingly, the chart in Fig. 8 (b), which reports the number of times each variables block is optimized by the MBI update rule, pinpoints that the frequency optimization plays a crucial role in the process of maximizing the SINR. This result is markedly different from the previous case, where an increase in SINR was primarily achieved by optimizing the code and the filter. Therefore, in this case study, the proposed transceiver design takes full advantage of the FDA-MIMO DOFs to suppress signal-dependent interference and improve the SINR.

Again, the squared modulus (dB) of the filter response (38) as a function of range-azimuth position, computed with the nominal parameters as well as with the optimized ones at 4-th, 100-th and final iterations, is reported in Figs. 9(a)-(d), respectively. It is possible to observe an effective clutter suppression, in both range and azimuth domains, achieved with the devised optimization strategy, which is better and better as the number of iterations increases.

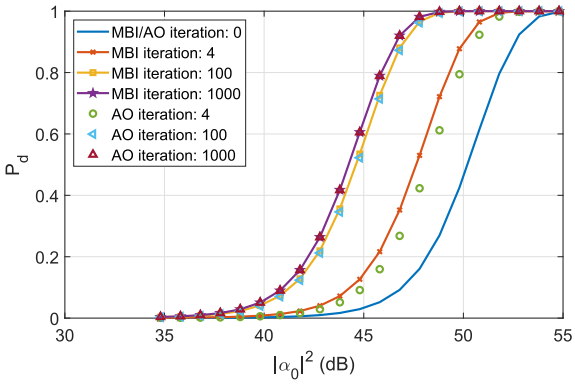

Fig. 10. Detection probability at a given iteration for the second environmental scenario.

As a last analysis for the considered clutter profile, the P_d (40) versus $|\alpha_0|^2$ is displayed in Fig. 10 using the SINR value attained by the devised approaches at several iterations of the corresponding optimization procedure, i.e., MM-MBI. An increase of P_d is connected with a large number of iterations, due to the increased SINR improvement. Like the previous case, after 4 iterations the MM-MBI yields a slight performance improvement w.r.t. the MM-AO, with a gap between curves less than 1 dB at $P_d = 0.9$. Still, the discrepancy between the two methods decreases with the iterations, eventually attaining the same result after 1000 iterations.

V. Conclusion

This paper has addressed the problem of joint transmitter and receiver design of a FDA-MIMO radar system with uniform frequency increment, operating in a signal-dependent interference environment. The goal is to maximize the SINR at the receiver end by optimizing both the transmit parameters, i.e., frequency increment and radar code, and the receive filter under some system constraints ruled by the available radar bandwidth, code features and limited transmitted energy. To provide a good-quality solution to the resulting non-convex NP-hard optimization problem, an iterative solution strategy based on the MM-MBI framework has been developed, where,

at each iteration, three subproblems, aimed at optimizing the receive filter, radar code, and frequency increment, respectively, are solved either optimally or resorting to the MM framework. Thereafter, the variable block related to the highest local SINR increment is updated according to the MBI rule, until a convergence condition is attained. The theoretical proof of the proposed algorithm's convergence property, in terms of satisfying the KKT condition, has been provided, along with details on its computational complexity.

Numerical results have been presented to underscore the performance of the devised joint transmitter and receiver optimization scheme in terms of SINR versus the number of iterations, detection probability, and signal-dependent interference cancellation capabilities at the filter output. The results have highlighted the effective SINR gain and the successful suppression of the signal-dependent clutter. Moreover, comparisons with counterparts including MM-AO, simpler MBI-based strategies, and the MBI-based algorithm in [35] (also initialized with the outcomes of the proposed MM-MBI) are also considered to further corroborate the improvements achievable via the proposed algorithm.

Possible future work might consider the validation of the devised optimization strategy with measured radar data collected under different environmental conditions as well as the extension of the framework to account for multiple pulses so as to allow a Space-Time Adaptive Processing (STAP).

APPENDIX

A. Proof of Proposition 1

To begin with, let us introduce two auxiliary variables $\boldsymbol{x} = \boldsymbol{b}_0(\Delta f)$ and $z = \sum_{k=1}^{K} \boldsymbol{b}_k^{\dagger}(\Delta f)\boldsymbol{\Sigma}_k{}^{(n-1)}\boldsymbol{b}_k(\Delta f) + \sigma_n^2 > 0$, so that the objective function in $\mathcal{P}_{\Delta f^{(n)}}$ can be rewritten in terms of $\boldsymbol{x}$ and z as

$$\mathrm{SINR}(\Delta f) = \left.\frac{\boldsymbol{x}^{\dagger}\boldsymbol{W}^{(n-1)}\boldsymbol{x}}{z}\right|_{\substack{\boldsymbol{x}=\boldsymbol{b}_0(\Delta f) \\ z=\sum_{k=1}^{K}\boldsymbol{b}_k^{\dagger}(\Delta f)\boldsymbol{\Sigma}_k{}^{(n-1)}\boldsymbol{b}_k(\Delta f)+\sigma_n^2}}, \tag{41}$$

where $\boldsymbol{W}^{(n-1)} = \boldsymbol{W}\left(\boldsymbol{w}^{(n-1)}, \boldsymbol{c}^{(n-1)}\right)$ and $\boldsymbol{\Sigma}_k{}^{(n-1)} = \boldsymbol{\Sigma}_k\left(\boldsymbol{w}^{(n-1)}, \boldsymbol{c}^{(n-1)}\right)$ are used for ease of notation.

Let us now observe that $\mathrm{SINR}(\Delta f)$ is jointly convex w.r.t. $\boldsymbol{x}$ and z. Hence, letting $\mathrm{SINR}(\boldsymbol{x}, z) = \frac{\boldsymbol{x}^{\dagger}\boldsymbol{W}^{(n-1)}\boldsymbol{x}}{z}$, $\boldsymbol{x} \in \mathbb{C}^M$, $z > 0$, and considering its first order Taylor expansion around $(\boldsymbol{x}_0, z_0)$, the following inequality holds

$$\mathrm{SINR}(\boldsymbol{x}, z) \geq \mathrm{SINR}_a(\boldsymbol{x}, z|\boldsymbol{x}_0, z_0), \tag{42}$$

where

$$\begin{aligned}\mathrm{SINR}_a(\boldsymbol{x}, z|\boldsymbol{x}_0, z_0) = {} & \frac{\boldsymbol{x}_0^{\dagger}\boldsymbol{W}^{(n-1)}\boldsymbol{x}_0}{z_0} \\ & + 2\Re\left\{\frac{\left(\boldsymbol{W}^{(n-1)}\boldsymbol{x}_0\right)^{\dagger}}{z_0}[\boldsymbol{x}-\boldsymbol{x}_0]\right\} \\ & - \frac{\boldsymbol{x}_0^{\dagger}\boldsymbol{W}^{(n-1)}\boldsymbol{x}_0}{z_0^2}[z-z_0]\end{aligned} \tag{43}$$

with equality if $\boldsymbol{x} = \boldsymbol{x}_0$ and $z = z_0$.

Therefore, by choosing $\boldsymbol{x}_0 = \boldsymbol{b}_0(\Delta f^{(n-1)})$ and $z_0 = \sum_{k=1}^{K} \boldsymbol{b}_k^{\dagger}(\Delta f_0)\boldsymbol{\Sigma}_k^{(n-1)}\boldsymbol{b}_k(\Delta f_0) + \sigma_n^2$, yields

$$\begin{aligned}\mathrm{SINR}(\Delta f) &= \mathrm{SINR}(\boldsymbol{x}, z)\Big|_{\substack{\boldsymbol{x}=\boldsymbol{b}_0(\Delta f) \\ z=\sum_{k=1}^{K}\boldsymbol{b}_k^{\dagger}(\Delta f)\boldsymbol{\Sigma}_k{}^{(n-1)}\boldsymbol{b}_k(\Delta f)+\sigma_n^2}} \\ &\geq \mathrm{SINR}_a(\boldsymbol{x}, z|\boldsymbol{x}_0, z_0)\Big|_{\substack{\boldsymbol{x}_0=\boldsymbol{b}_0(\Delta f^{(n-1)}) \\ z_0=\sum_{k=1}^{K}\boldsymbol{b}_k^{\dagger}(\Delta f_0)\boldsymbol{\Sigma}_k^{(n-1)}\boldsymbol{b}_k(\Delta f_0)+\sigma_n^2}} \\ &= \mathrm{SINR}_a\left(\Delta f|\Delta f^{(n-1)}, \boldsymbol{w}^{(n-1)}, \boldsymbol{c}^{(n-1)}\right),\end{aligned} \tag{44}$$

where

$$\begin{aligned}&\mathrm{SINR}_a\left(\Delta f|\Delta f^{(n-1)}, \boldsymbol{w}^{(n-1)}, \boldsymbol{c}^{(n-1)}\right) \\ &= \sum_{k=1}^{K} \boldsymbol{b}_k^{\dagger}(\Delta f)\boldsymbol{A}_k^{(n-1)}\boldsymbol{b}_k(\Delta f) + 2\Re\left\{\boldsymbol{h}_0^{\dagger}\boldsymbol{b}_0(\Delta f)\right\} + U,\end{aligned} \tag{45}$$

with

- $\boldsymbol{A}_k^{(n-1)} = -\frac{\boldsymbol{x}_0^{\dagger}\boldsymbol{W}^{(n-1)}\boldsymbol{x}_0}{z_0^2}\boldsymbol{\Sigma}_k^{(n-1)} \in \mathbb{C}^{M\times M}$;
- $\boldsymbol{h}_0 = \frac{\boldsymbol{W}^{(n-1)}\boldsymbol{x}_0}{z_0} \in \mathbb{C}^M$;
- $U = -\frac{\sigma_n^2\boldsymbol{x}_0^{\dagger}\boldsymbol{W}^{(n-1)}\boldsymbol{x}_0}{z_0^2}$.

Then, using the Taylor expansion with Lagrange remainder yields

$$\begin{aligned}&\boldsymbol{b}_k^{\dagger}(\Delta f)\boldsymbol{A}_k^{(n-1)}\boldsymbol{b}_k(\Delta f) \\ &= \boldsymbol{b}_k^{\dagger}(\Delta f^{(n-1)})\boldsymbol{A}_k^{(n-1)}\boldsymbol{b}_k(\Delta f^{(n-1)}) \\ &\quad + \frac{\partial}{\partial\Delta f}\left[\boldsymbol{b}_k^{\dagger}(\Delta f)\boldsymbol{A}_k^{(n-1)}\boldsymbol{b}_k(\Delta f)\right]\Big|_{\Delta f=\Delta f^{(n-1)}} \\ &\quad \left(\Delta f - \Delta f^{(n-1)}\right) + \frac{1}{2}\left(\Delta f - \Delta f^{(n-1)}\right)^2\lambda_k^{(n-1)},\end{aligned} \tag{46}$$

where

$$\begin{aligned}&\frac{\partial}{\partial\Delta f}\left[\boldsymbol{b}_k^{\dagger}(\Delta f)\boldsymbol{A}_k^{(n-1)}\boldsymbol{b}_k(\Delta f)\right]\Big|_{\Delta f=\Delta f^{(n-1)}} \\ &= 2\Re\left\{\dot{\boldsymbol{b}}_k^{\dagger}(\Delta f^{(n-1)})\boldsymbol{A}_k^{(n-1)}\boldsymbol{b}_k(\Delta f^{(n-1)})\right\}\end{aligned} \tag{47}$$

with

$$\begin{aligned}\dot{\boldsymbol{b}}_k(\Delta f^{(n-1)}) &= \left.\frac{\partial\boldsymbol{b}_k(\Delta f)}{\partial\Delta f}\right|_{\Delta f=\Delta f^{(n-1)}} \\ &= j2\pi\Delta\tau_k\boldsymbol{E}_{\mathrm{T}}\boldsymbol{b}_k(\Delta f^{(n-1)}) \in \mathbb{C}^M,\end{aligned} \tag{48}$$

$\boldsymbol{E}_{\mathrm{T}} = \mathrm{diag}([0, 1, \cdots, M-1]^{\mathrm{T}}) \in \mathbb{C}^{M\times M}$, while $\lambda_k^{(n-1)}$ denotes the derivative of $\frac{\partial}{\partial\Delta f}\left[\boldsymbol{b}_k^{\dagger}(\Delta f)\boldsymbol{A}_k^{(n-1)}\boldsymbol{b}_k(\Delta f)\right]$ evaluated at $\Delta f = \zeta_\Delta$ (with ζ_Δ between $\Delta f^{(n-1)}$ and Δf), which is given by

$$\begin{aligned}\lambda_k^{(n-1)} &= \left.\frac{\partial^2\left[\boldsymbol{b}_k^{\dagger}(\Delta f)\boldsymbol{A}_k^{(n-1)}\boldsymbol{b}_k(\Delta f)\right]}{\partial^2\Delta f}\right|_{\Delta f=\zeta_\Delta} \\ &= 2\left.\frac{\partial\Re\left\{\dot{\boldsymbol{b}}_k^{\dagger}(\Delta f)\boldsymbol{A}_k^{(n-1)}\boldsymbol{b}_k(\Delta f)\right\}}{\partial\Delta f}\right|_{\Delta f=\zeta_\Delta} \\ &= 2\Re\left\{\ddot{\boldsymbol{b}}_k^{\dagger}(\zeta_\Delta)\boldsymbol{A}_k^{(n-1)}\boldsymbol{b}_k(\zeta_\Delta) + \dot{\boldsymbol{b}}_k^{\dagger}(\zeta_\Delta)\boldsymbol{A}_k^{(n-1)}\dot{\boldsymbol{b}}_k(\zeta_\Delta)\right\} \\ &= 2\Re\left\{-4\pi^2\Delta\tau_k^2\boldsymbol{b}_k^{\dagger}(\zeta_\Delta)\boldsymbol{E}_{\mathrm{T}}^{2\dagger}\boldsymbol{A}_k^{(n-1)}\boldsymbol{b}_k(\zeta_\Delta)\right.\end{aligned}$$

$$
\begin{aligned}
&+4\pi^2\Delta\tau_k^2\boldsymbol{b}_k^\dagger(\zeta_\Delta)\boldsymbol{E}_{\mathrm{T}}^\dagger\boldsymbol{A}_k^{(n-1)}\boldsymbol{E}_{\mathrm{T}}\boldsymbol{b}_k(\zeta_\Delta)\Big\}\\
&=8\pi^2\Delta\tau_k^2\Re\Big\{\boldsymbol{b}_k^\dagger(\zeta_\Delta)\boldsymbol{E}_{\mathrm{T}}^\dagger\boldsymbol{A}_k^{(n-1)}\boldsymbol{E}_{\mathrm{T}}\boldsymbol{b}_k(\zeta_\Delta)\\
&\quad-\boldsymbol{b}_k^\dagger(\zeta_\Delta)\boldsymbol{E}_{\mathrm{T}}^{2\dagger}\boldsymbol{A}_k^{(n-1)}\boldsymbol{b}_k(\zeta_\Delta)\Big\}\\
&=8\pi^2\Delta\tau_k^2\Re\Big\{\boldsymbol{b}_k^\dagger(\zeta_\Delta)\Big[\boldsymbol{E}_{\mathrm{T}}^\dagger\boldsymbol{A}_k^{(n-1)}\boldsymbol{E}_{\mathrm{T}}-\boldsymbol{E}_{\mathrm{T}}^{2\dagger}\boldsymbol{A}_k^{(n-1)}\Big]\boldsymbol{b}_k(\zeta_\Delta)\Big\}\\
&=8\pi^2\Delta\tau_k^2\Re\Big\{\boldsymbol{b}_k^\dagger(\zeta_\Delta)\bar{\boldsymbol{A}}_{\boldsymbol{E}}\boldsymbol{b}_k(\zeta_\Delta)\Big\},
\end{aligned}
\tag{49}
$$

where

- $\ddot{\boldsymbol{b}}_k(\zeta_\Delta)=\left.\frac{\partial\dot{\boldsymbol{b}}_k(\Delta f)}{\partial\Delta f}\right|_{\Delta f=\zeta_\Delta}=-4\pi^2\Delta\tau_k^2\boldsymbol{E}_{\mathrm{T}}^2\boldsymbol{b}_k(\zeta_\Delta)\in\mathbb{C}^M$;
- $\bar{\boldsymbol{A}}_{\boldsymbol{E}}=\boldsymbol{E}_{\mathrm{T}}^\dagger\boldsymbol{A}_k^{(n-1)}\boldsymbol{E}_{\mathrm{T}}-\boldsymbol{E}_{\mathrm{T}}^{2\dagger}\boldsymbol{A}_k^{(n-1)}\in\mathbb{C}^{M\times M}$.

Moreover, since

$$
\begin{aligned}
\Re\Big\{\boldsymbol{b}_k^\dagger(\zeta_\Delta)\bar{\boldsymbol{A}}_{\boldsymbol{E}}\boldsymbol{b}_k(\zeta_\Delta)\Big\}&=\sqrt{M}\Re\left\{\boldsymbol{b}_k^\dagger(\zeta_\Delta)\bar{\boldsymbol{A}}_{\boldsymbol{E}}\frac{\boldsymbol{b}_k(\zeta_\Delta)}{\|\boldsymbol{b}_k(\zeta_\Delta)\|}\right\}\\
&\geq-\sqrt{M}\left|\boldsymbol{b}_k^\dagger(\zeta_\Delta)\bar{\boldsymbol{A}}_{\boldsymbol{E}}\boldsymbol{l}_m\right|\\
&\geq-\sqrt{M}\left\|\boldsymbol{b}_k^\dagger(\zeta_\Delta)\bar{\boldsymbol{A}}_{\boldsymbol{E}}\right\|,
\end{aligned}
\tag{50}
$$

where $\boldsymbol{l}_m=\frac{\boldsymbol{b}_k(\zeta_\Delta)}{\|\boldsymbol{b}_k(\zeta_\Delta)\|}$ with $\|\boldsymbol{l}_m\|^2=1$, the first term in (45) can be tightly lower bounded as

$$
\begin{aligned}
\lambda_k^{(n-1)}&=8\pi^2\Delta\tau_k^2\Re\Big\{\boldsymbol{b}_k^\dagger(\zeta_\Delta)\bar{\boldsymbol{A}}_{\boldsymbol{E}}\boldsymbol{b}_k(\zeta_\Delta)\Big\}\\
&\geq-8\pi^2\Delta\tau_k^2\sqrt{M}\left\|\boldsymbol{b}_k^\dagger(\zeta_\Delta)\bar{\boldsymbol{A}}_{\boldsymbol{E}}\right\|=\tilde{\lambda}_k^{(n-1)}.
\end{aligned}
\tag{51}
$$

Now, the second term in (45) can be further expressed as

$$
\begin{aligned}
&2\Re\Big\{\boldsymbol{h}_0^\dagger\boldsymbol{b}_0(\Delta f)\Big\}\\
&=2\Re\left\{\sum_{m=1}^M h_0^*(m)e^{j2\pi\Delta\tau_0(m-1)\Delta f}\right\}\\
&=2\sum_{m=1}^M|h_0(m)|\cos(2\pi\Delta\tau_0(m-1)\Delta f-\arg(h_0(m)))\\
&=\sum_{m=1}^M g_m\cos(2\pi\Delta\tau_0(m-1)\Delta f+\varphi_m),
\end{aligned}
\tag{52}
$$

where $g_m=2|h_0(m)|$ and $\varphi_m=-\arg(h_0(m))$ with $h_0(m)$ the m-th ($m=1,\cdots,M$) element of $\boldsymbol{h}_0$.

Hence, leveraging again the first order Taylor expansion with Lagrange reminder, it yields,

$$
\begin{aligned}
&2\Re\Big\{\boldsymbol{h}_0^\dagger\boldsymbol{b}_0(\Delta f)\Big\}\\
&\geq\sum_{m=1}^M g_m\cos\big(2\pi\Delta\tau_0(m-1)\Delta f^{(n-1)}+\varphi_m\big)\\
&\quad-\sum_{m=1}^M g_m2\pi\Delta\tau_0(m-1)\sin\big(2\pi\Delta\tau_0(m-1)\Delta f^{(n-1)}+\varphi_m\big)\\
&\quad\big(\Delta f-\Delta f^{(n-1)}\big)-\frac{1}{2}\sum_{m=1}^M g_m(2\pi\Delta\tau_0(m-1))^2\\
&\quad\big(\Delta f-\Delta f^{(n-1)}\big)^2.
\end{aligned}
\tag{53}
$$

Summarizing,

$$
\begin{aligned}
\mathrm{SINR}(\Delta f)&\geq X^{(n-1)}\big(\Delta f-\Delta f^{(n-1)}\big)^2\\
&\quad+\hat{X}^{(n-1)}\big(\Delta f-\Delta f^{(n-1)}\big)+\bar{X}^{(n-1)}\\
&=X^{(n-1)}\Delta f^2+\dot{\hat{X}}^{(n-1)}\Delta f+\ddot{\hat{X}}^{(n-1)},
\end{aligned}
\tag{54}
$$

where

- $X^{(n-1)}=\frac{1}{2}\sum_{k=1}^K\tilde{\lambda}_k^{(n-1)}-\frac{1}{2}\sum_{m=1}^M g_m(2\pi\Delta\tau_0(m-1))^2$;
- $\hat{X}^{(n-1)}=2\sum_{k=1}^K\Re\Big\{\dot{\boldsymbol{b}}_k^\dagger(\Delta f^{(n-1)})\boldsymbol{A}_k^{(n-1)}\boldsymbol{b}_k(\Delta f^{(n-1)})\Big\}-\sum_{m=1}^M g_m2\pi\Delta\tau_0(m-1)\sin\big(2\pi\Delta\tau_0(m-1)\Delta f^{(n-1)}+\varphi_m\big)$;
- $\bar{X}^{(n-1)}=\sum_{k=1}^K\boldsymbol{b}_k^\dagger\big(\Delta f^{(n-1)}\big)\boldsymbol{A}_k^{(n-1)}\boldsymbol{b}_k\big(\Delta f^{(n-1)}\big)+\sum_{m=1}^M g_m\cos\big(2\pi\Delta\tau_0(m-1)\Delta f^{(n-1)}+\varphi_m\big)+U$;
- $\dot{\hat{X}}^{(n-1)}=-2X^{(n-1)}\Delta f^{(n-1)}+\hat{X}^{(n-1)}$;
- $\ddot{\hat{X}}^{(n-1)}=X^{(n-1)}\big(\Delta f^{(n-1)}\big)^2-\hat{X}^{(n-1)}\Delta f^{(n-1)}+\bar{X}^{(n-1)}$.

As a consequence,

$$
\begin{aligned}
&\widehat{\mathrm{SINR}}_a\big(\Delta f|\Delta f^{(n-1)},\boldsymbol{w}^{(n-1)},\boldsymbol{c}^{(n-1)}\big)\\
&\quad=X^{(n-1)}\Delta f^2+\dot{\hat{X}}^{(n-1)}\Delta f+\ddot{\hat{X}}^{(n-1)},
\end{aligned}
\tag{55}
$$

is a surrogate (tight minorant) to the objective function $\mathrm{SINR}(\Delta f)$.

B. Proof of Proposition 2

The solution $y_3^\star$ to the problem $\mathcal{P}_{y_3^{(n)}}$ is obtained as

$$
y_3^\star=\arg\max_{0<y_3\leq B_w/(M-1)}\big(X^{(n-1)}y_3^2+\dot{\hat{X}}^{(n-1)}y_3+\ddot{\hat{X}}^{(n-1)}\big).
\tag{56}
$$

It is worth noting that assuming $X^{(n-1)}<0$, the objective function in (56) is strictly concave[4] in y_3, so the optimal solution is given by

$$
\hat{y}_3=\max(\min(\tilde{y}_3,B_w/(M-1)),0)
\tag{57}
$$

with

$$
\tilde{y}_3=-\frac{\dot{\hat{X}}^{(n-1)}}{2X^{(n-1)}}.
\tag{58}
$$

C. Proof of Proposition 3

The proof exploits the same procedure as in Appendix F of [35], where the only difference is that, the feasible set to $\mathcal{P}$ is expressed as

$$
\mathcal{F}=\mathcal{A}\times\mathcal{B}\times\mathcal{C},
\tag{59}
$$

with $\mathcal{A}=\{\boldsymbol{y}_1:\|\boldsymbol{y}_1\|^2=1\}$, $\mathcal{B}=\{\boldsymbol{y}_2:\|\boldsymbol{y}_2\|^2=1,\|\boldsymbol{y}_2-\boldsymbol{c}_0\|^2\leq\delta\}$, and $\mathcal{C}=\{y_3:0\leq y_3\leq B_w/(M-1)\}$.

REFERENCES

[1] B. Tang, J. Tuck, and P. Stoica, "Polyphase waveform design for MIMO radar space time adaptive processing," *IEEE Trans. Signal Process.*, vol. 68, pp. 2143–2154, 2020.

[2] C.-Y. Chen and P. P. Vaidyanathan, "MIMO radar waveform optimization with prior information of the extended target and clutter," *IEEE Trans. Signal Process.*, vol. 57, no. 9, pp. 3533–3544, Sep. 2009.

[3] P. Stoica, H. He, and J. Li, "Optimization of the receive filter and transmit sequence for active sensing," *IEEE Trans. Signal Process.*, vol. 60, no. 4, pp. 1730–1740, Apr. 2012.

[4] If $X^{(n-1)}$ is not smaller than 0, then the the objective function in (56) is only concave.

[4] A. Aubry, A. De Maio, A. Farina, and M. Wicks, "Knowledge-aided (potentially cognitive) transmit signal and receive filter design in signal-dependent clutter," *IEEE Trans. Aerosp. Electron. Syst.*, vol. 49, no. 1, pp. 93–117, Jan. 2013.

[5] A. Aubry, A. De Maio, M. A. Govoni, and L. Martino, "On the design of multi-spectrally constrained constant modulus radar signals," *IEEE Trans. Signal Process.*, vol. 68, pp. 2231–2243, 2020.

[6] G. Cui, A. De Maio, A. Farina, and J. Li, *Radar Waveform Design Based on Optimization Theory*. Edison, NJ, USA: IET/SciTech, 2020.

[7] A. De Maio, S. De Nicola, Y. Huang, S. Zhang, and A. Farina, "Code design to optimize radar detection performance under accuracy and similarity constraints," *IEEE Trans. Signal Process.*, vol. 56, no. 11, pp. 5618–5629, Nov. 2008.

[8] A. De Maio, S. De Nicola, Y. Huang, Z.-Q. Luo, and S. Zhang, "Design of phase codes for radar performance optimization with a similarity constraint," *IEEE Trans. Signal Process.*, vol. 57, no. 2, pp. 610–621, Feb. 2009.

[9] O. Aldayel, V. Monga, and M. Rangaswamy, "Successive QCQP refinement for MIMO radar waveform design under practical constraints," *IEEE Trans. Signal Process.*, vol. 64, no. 14, pp. 3760–3774, Jul. 2016.

[10] X. Du, A. Aubry, A. De Maio, and G. Cui, "Hidden convexity in robust waveform and receive filter bank optimization under range unambiguous clutter," *IEEE Signal Process. Lett.*, vol. 27, pp. 885–889, 2020.

[11] L. Wu, P. Babu, and D. P. Palomar, "Transmit waveform/receive filter design for MIMO radar with multiple waveform constraints," *IEEE Trans. Signal Process.*, vol. 66, no. 6, pp. 1526–1540, Mar. 2018.

[12] H. He, P. Stoica, and J. Li, "Designing unimodular sequence sets with good correlations—Including an application to MIMO radar," *IEEE Trans. Signal Process.*, vol. 57, no. 11, pp. 4391–4405, Nov. 2009.

[13] A. Aubry, A. De Maio, and M. M. Naghsh, "Optimizing radar waveform and Doppler filter bank via generalized fractional programming," *IEEE J. Sel. Topics Signal Process.*, vol. 9, no. 8, pp. 1387–1399, Dec. 2015.

[14] M. Deng, Z. Cheng, and Z. He, "Limited-memory receive filter design for massive MIMO radar in signal-dependent interference," *IEEE Signal Process. Lett.*, vol. 29, pp. 1536–1540, 2022.

[15] C. Shi, Y. Li, and R. Tao, "Spatial slow-time waveform and adaptive receive filter design for MIMO radar," in *Proc. IEEE Radar Conf. (RadarConf22)*, New York City, NY, USA, Mar. 2022, pp. 1–6.

[16] M. M. Feraidooni, D. Gharavian, M. Alaee-Kerahroodi, and S. Imani, "A coordinate descent framework for probing signal design in cognitive MIMO radars," *IEEE Commun. Lett.*, vol. 24, no. 5, pp. 1115–1118, May 2020.

[17] J. Yang, A. Aubry, A. De Maio, X. Yu, and G. Cui, "Multi-spectrally constrained transceiver design against signal-dependent interference," *IEEE Trans. Signal Process.*, vol. 70, pp. 1320–1332, 2022.

[18] P. Antonik, M. C. Wicks, H. D. Griffiths, and C. J. Baker, "Frequency diverse array radars," in *Proc. IEEE Conf. Radar*, Verona, NY, USA, Mar. 2006, pp. 1–3.

[19] L. Lan et al., "GLRT-based adaptive target detection in FDA-MIMO radar," *IEEE Trans. Aerosp. Electron. Syst.*, vol. 57, no. 1, pp. 597–613, Feb. 2021.

[20] A. Basit, W. Khan, S. Khan, and I. M. Qureshi, "Development of frequency diverse array radar technology: A review," *IET Radar, Sonar Navigat.*, vol. 12, no. 2, pp. 165–175, Feb. 2018.

[21] L. Lan, G. Liao, J. Xu, S. Zhu, C. Zeng, and Y. Zhang, "Control and utilization of range-dependent beampattern with waveform diverse array radars," *Chin. J. Aeronaut.*, vol. 35, no. 12, pp. 1–31, Dec. 2022.

[22] P. F. Sammartino, C. J. Baker, and H. D. Griffiths, "Frequency diverse MIMO techniques for radar," *IEEE Trans. Aerosp. Electron. Syst.*, vol. 49, no. 1, pp. 201–222, Jan. 2013.

[23] L. Lan, M. Rosamilia, A. Aubry, A. De Maio, and G. Liao, "Single-snapshot angle and incremental range estimation for FDA-MIMO radar," *IEEE Trans. Aerosp. Electron. Syst.*, vol. 57, no. 6, pp. 3705–3718, Dec. 2021.

[24] L. Lan, J. Xu, G. Liao, Y. Zhang, F. Fioranelli, and H. C. So, "Suppression of mainbeam deceptive jammer with FDA-MIMO radar," *IEEE Trans. Veh. Technol.*, vol. 69, no. 10, pp. 11584–11598, Oct. 2020.

[25] J. Xu, G. Liao, and H. C. So, "Space-time adaptive processing with vertical frequency diverse array for range-ambiguous clutter suppression," *IEEE Trans. Geosci. Remote Sens.*, vol. 54, no. 9, pp. 5352–5364, Sep. 2016.

[26] C. Wang, J. Xu, G. Liao, X. Xu, and Y. Zhang, "A range ambiguity resolution approach for high-resolution and wide-swath SAR imaging using frequency diverse array," *IEEE J. Sel. Topics Signal Process.*, vol. 11, no. 2, pp. 336–346, Mar. 2017.

[27] W. Xu, L. Zhang, H. Bi, P. Huang, and W. Tan, "FDA beampattern synthesis with both nonuniform frequency offset and array spacing," *IEEE Antennas Wireless Propag. Lett.*, vol. 20, no. 12, pp. 2354–2358, Dec. 2021.

[28] W. Khan, I. M. Qureshi, and S. Saeed, "Frequency diverse array radar with logarithmically increasing frequency offset," *IEEE Antennas Wireless Propag. Lett.*, vol. 14, pp. 499–502, 2015.

[29] Y. Liao, J. Wang, and Q. H. Liu, "Transmit beampattern synthesis for frequency diverse array with particle swarm frequency offset optimization," *IEEE Trans. Antennas Propag.*, vol. 69, no. 2, pp. 892–901, Feb. 2021.

[30] W. Jia, W.-Q. Wang, and S. Zhang, "Joint design of the transmit and receive weights for coherent FDA radar," *Signal Process.*, vol. 204, Mar. 2023, Art. no. 108834.

[31] N. Rubinstein and J. Tabrikian, "Frequency diverse array signal optimization: From non-cognitive to cognitive radar," *IEEE Trans. Signal Process.*, vol. 69, pp. 6206–6220, 2021.

[32] C. Zhou, C. Wang, J. Gong, M. Tan, L. Bao, and M. Liu, "Joint optimisation of transmit beamspace and receive filter in frequency diversity array-multi-input multi-output radar," *IET Radar, Sonar Navigat.*, vol. 16, no. 12, pp. 2031–2039, Dec. 2022.

[33] Z. Ding and J. Xie, "Joint transmit and receive beamforming for cognitive FDA-MIMO radar with moving target," *IEEE Sensors J.*, vol. 21, no. 18, pp. 20878–20885, Sep. 2021.

[34] J. Cheng, M. Juhlin, A. Jakobsson, and W.-Q. Wang, "Designing optimal frequency offsets for frequency diverse array MIMO radar," *IEEE Trans. Aerosp. Electron. Syst.*, vol. 59, no. 6, pp. 8104–8118, Dec. 2023.

[35] L. Lan, M. Rosamilia, A. Aubry, A. De Maio, and G. Liao, "FDA-MIMO transmitter and receiver optimization," *IEEE Trans. Signal Process.*, vol. 72, pp. 1576–1589, 2024.

[36] D. P. Bertsekas, *Nonlinear Programming*, 2nd ed. Belmont, MA, USA: Athena Scientific, 1999.

[37] A. Aubry, A. De Maio, A. Zappone, M. Razaviyayn, and Z.-Q. Luo, "A new sequential optimization procedure and its applications to resource allocation for wireless systems," *IEEE Trans. Signal Process.*, vol. 66, no. 24, pp. 6518–6533, Dec. 2018.

[38] M. Razaviyayn, M. Hong, and Z.-Q. Luo, "A unified convergence analysis of block successive minimization methods for nonsmooth optimization," *SIAM J. Optim.*, vol. 23, no. 2, pp. 1126–1153, Jan. 2013.

[39] A. Aubry, P. Babu, A. De Maio, G. Fatima, and N. Sahu, "A robust framework to design optimal sensor locations for TOA or RSS source localization techniques," *IEEE Trans. Signal Process.*, vol. 71, pp. 1293–1306, 2023.

[40] J. C. Chen, H. C. Lai, and S. Schaible, "Complex fractional programming and the charnes-cooper transformation," *J. Optim. Theory Appl.*, vol. 126, no. 1, pp. 203–213, Jul. 2005.

[41] W. Ai, Y. Huang, and S. Zhang, "New results on Hermitian matrix rank-one decomposition," *Math. Program.*, vol. 128, nos. 1–2, pp. 253–283, Aug. 2009.

[42] H. L. Van Trees, *Optimum Array Processing: Part IV, Detection, Estimation, and Modulation Theory*. Hoboken, NJ, USA: Wiley, 2004.

[43] J. R. Guerci, *Cognitive Radar, The Knowledge-aided Fully Adaptive Approach*. Norwood, MA, USA: Artech House, 2010.

[44] A. Farina, A. De Maio, and S. Haykin, *The Impact of Cognition on Radar Technology, Radar, Sonar & Navigation*. Stevenage, U.K.: Institution of Engineering and Technology, 2017.

[45] A. Ben-Tal and A. Nemirovski, *Lecture on Modern Convex Optimization: Analysis, Algorithms, and Engineering Applications*. Philadelphia, PA, USA: MPS-SIAM, 2001.

[46] J. R. Shewchuk, "An introduction to the conjugate gradient method without the agonizing pain," School Comput. Sci., Carnegie Mellon Univ., Pittsburgh, PA, USA, Tech. Rep. CMU-CS-94-125, 1994.

[47] J. Marcum, "A statistical theory of target detection by pulsed radar," *IEEE Trans. Inf. Theory*, vol. IT-6, no. 2, pp. 59–267, Apr. 1960.

[48] R. T. Rockafellar, *Convex Analysis*. Princeton, NJ, USA: Princeton Univ. Press, 1970.

[49] H. H. Bauschke and P. L. Combettes, *Convex Analysis and Monotone Operator Theory in Hilbert Spaces*. New York, NY, USA: Springer, 2011.

Lan Lan (Member, IEEE) was born in Xi'an, China, in 1993. She received the B.S. degree in electronic engineering and the Ph.D. degree in signal and information processing from Xidian University, Xi'an, in 2015 and 2020, respectively. From July 2019 to July 2020, she was a Visiting Ph.D. Student with the University of Naples Federico II, Naples, Italy. She is currently an Associate Professor with the National Key Laboratory of Radar Signal Processing, Xidian University. Her research interests include frequency diverse array radar systems, MIMO radar signal processing, target detection, and ECCM.

She was elected as the Youth Elite Scientist Sponsorship Program by China Association for Science and Technology in 2022 and the XXXV-th URSI Young Scientists Award in 2023. She is a TPC Member and the Session Chair of important conferences, including the ICASSP, IEEE Radar Conference, International Conference on Radar, and IEEE SAM. She is on the Editorial Board of *Digital Signal Processing*.

Massimo Rosamilia (Member, IEEE) received the B.S. (Hons.) and M.S. degrees in computer engineering from the University of Salerno, Fisciano, Italy, in 2017 and 2019, respectively, and the Ph.D. degree (cum Laude) in information technologies and electrical engineering from the University of Naples Federico II, Naples, Italy, in 2023. From September to November 2021, he was a Visiting Ph.D. Student with Cranfield University, Shrivenham, U.K.; and the University of Luxembourg, Luxembourg, from September 2022 to December 2022. He is currently a Researcher with the University of Naples Federico II. His research interest lies in the field of statistical signal processing, with an emphasis on radar signal processing. He ranked second in the Student Contest of the first International Virtual School on Radar Signal Processing in 2020. In 2023, he has coauthored the paper winning the SET Panel Best Paper Award (Young Scientist) at the NATO SET-319 Specialists' Meeting on "New Mathematical Frontiers for Multi-Dimensional Radar Systems." He also received the GTTI Ph.D. Award for the Ph.D. Theses in the field of Communication Technologies.

Augusto Aubry (Senior Member, IEEE) received the Dr.-Eng. degree (Hons.) in telecommunication engineering and the Ph.D. degree in electronic and telecommunication engineering from the University of Naples Federico II, Naples, Italy, in 2007 and 2011, respectively. From February to April 2012, he was a Visiting Researcher with Hong Kong Baptist University, Hong Kong. He is currently an Associate Professor with the University of Naples Federico II. His research interests include statistical signal processing and optimization theory, with an emphasis on MIMO communications and radar signal processing. He was a co-recipient of the 2013 Best Paper Award (entitled to B. Carlton) of the IEEE TRANSACTIONS ON AEROSPACE AND ELECTRONIC SYSTEMS with the contribution "Knowledge-Aided (Potentially Cognitive) Transmit Signal and Receive Filter Design in Signal-Dependent Clutter." He was a recipient of the 2022 IEEE Fred Nathanson Memorial Award as the Young (less than 40 years of age) AESS Radar Engineer 2022, for the outstanding contributions to the application of modern optimization theory to radar waveform design and adaptive signal processing.

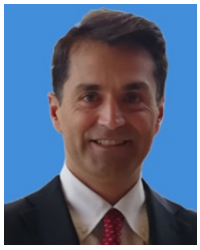

Antonio De Maio (Fellow, IEEE) received the Dr.-Eng. (Hons.) and Ph.D. degrees in information engineering from the University of Naples Federico II, Naples, Italy, in 1998 and 2002, respectively. From October to December 2004, he was a Visiting Researcher with the U.S. Air Force Research Laboratory, Rome, NY, USA; and The Chinese University of Hong Kong, Hong Kong, from November 2007 to December 2007. He is currently a Professor with the University of Naples Federico II. His research interest lies in the field of statistical signal processing, with an emphasis on radar detection, optimization theory applied to radar signal processing, and multiple-access communications.

He was a recipient of the 2010 IEEE Fred Nathanson Memorial Award as the Young (less than 40 years of age) AESS Radar Engineer 2010, whose performance was particularly noteworthy as evidenced by contributions to the radar art over a period of several years, with the following citation for "Robust CFAR Detection, Knowledge-Based Radar Signal Processing, and Waveform Design and Diversity." He was a co-recipient of the 2013 Best Paper Award (entitled to B. Carlton) of IEEE TRANSACTIONS ON AEROSPACE AND ELECTRONIC SYSTEMS with the contribution "Knowledge-Aided (Potentially Cognitive) Transmit Signal and Receive Filter Design in Signal-Dependent Clutter." He was also a recipient of the 2024 IEEE Warren White Award for outstanding achievements due to a major technical advance (or series of advances) in the art of radar engineering, with the citation "For Contributions to Radar Signal Processing Techniques for Target Detection, Waveform Design, and Electronic Protection."

Guisheng Liao (Senior Member, IEEE) was born in Guilin, Guangxi, China, in 1963. He received the B.S. degree in mathematics from Guangxi University, Guangxi, in 1985, and the M.S. degree in computer software and the Ph.D. degree in signal and information processing from Xidian University, Xi'an, China, in 1990 and 1992, respectively.

He is currently a Full Professor with the National Key Laboratory of Radar Signal Processing. He has been the first Dean of Hangzhou Institute of Technology, Xidian University, since 2021, where he was the Dean of the School of Electronic Engineering, from 2013 to 2021. He was a Senior Visiting Scholar with The Chinese University of Hong Kong, from 1999 to 2000. His research interests include array signal processing, space-time adaptive processing, radar waveform design, and airborne/space surveillance, and warning radar systems. He won the National Science Fund for Distinguished Young Scholars in 2008.

Open Access funding provided by 'Università degli Studi di Napoli "Federico II"' within the CRUI CARE Agreement